

Charged perfect fluid tori in strong central gravitational and dipolar magnetic fields

Jiří Kovář,^{*} Petr Slaný, Claudio Cremaschini, and Zdeněk Stuchlík

Institute of Physics and Research Centre of Theoretical Physics and Astrophysics, Faculty of Philosophy and Science, Silesian University in Opava, Bezručovo nám. 13, CZ-746 01 Opava, Czech Republic

Vladimír Karas and Audrey Trova

Astronomical Institute, Academy of Sciences, Boční II, CZ-141 31 Prague, Czech Republic

(Received 9 March 2016; published 21 June 2016)

We study electrically charged perfect fluid toroidal structures encircling a spherically symmetric gravitating object with Schwarzschild spacetime geometry and endowed with a dipole magnetic field. The work represents a direct continuation of our previous general-relativistic studies of electrically charged fluid in the approximation of zero conductivity, which formed tori around a Reissner-Nordström black hole or a Schwarzschild black hole equipped with a test electric charge and immersed in an asymptotically uniform magnetic field. After a general introduction of the zero-conductivity charged fluid model, we discuss a variety of possible topologies of the toroidal fluid configurations. Along with the charged equatorial tori forming interesting coupled configurations, we demonstrate the existence of the off-equatorial tori, for which the dipole type of magnetic field seems to be necessary. We focus on orbiting structures with constant specific angular momentum and on those in permanent rigid rotation. We stress that the general analytical treatment developed in our previous works is enriched here by the integrated form of the pressure equations. To put our work into an astrophysical context, we identify the central object with an idealization of a nonrotating magnetic neutron star. Constraining ranges of its parameters and also parameters of the circling fluid, we discuss a possible relevance of the studied toroidal structures, presenting along with their topology also pressure, density, temperature and charge profiles.

DOI: [10.1103/PhysRevD.93.124055](https://doi.org/10.1103/PhysRevD.93.124055)

I. INTRODUCTION

Investigation of astrophysical fluids represents one of the most challenging and important tasks in astrophysics. Encircling compact objects, the fluids manifest themselves in the compressible (gaseous-like) phase predominantly, in different regimes and scenarios: as a pure neutral or ionized gas—plasma (satisfying the typical quasi-neutrality and high-conductivity conditions), as a pure neutral or charged dust, and very often as a dispersed medium, such as dusty (grain) gas, dusty plasma, etc. The gaseous fluid can range from an extremely diluted case (represented as separated particles, well described within a test-particle approach [1–5]), through a diluted one (described within a kinetic approach [6–9]), up to the dense fluid (conveniently studied within a magnetohydrodynamic approach [10–12]). From another point of view, the fluid can be in dynamical situations (falling down onto the compact objects or being launched in the form of winds and jets) or settled down in an equilibrium configuration.

This paper deals with the last scenario, summarizing our results concerning a general-relativistic magnetohydrodynamic description of charged fluid equilibrium

configurations. We consider the perfect fluid approximation (no internal viscosity and friction—typical features of gaseous matter) and the dielectric (fully nonconductive) approximation of the fluid enhanced with a global nonzero electric charge. This approximation is directly opposite of the infinite-conductivity one, often applied in the standard, the so-called ideal, magnetohydrodynamic studies of plasma being typically highly conductive and with zero global charge. Our conception of the perfect dielectric fluid was introduced in the paper [13] for the first time, there being performed on the background of a Reissner-Nordström black hole.

Let us emphasize that we explore situations where both gravitational and electromagnetic effects play roles in their mutual interaction. While the strong gravity of a central body and the ambient electromagnetic field exert torques on the matter because of its moderate specific charge (typically like in the case of pressureless matter consisting of electrically charged and relatively extensive dust grains), also pressure terms are taken into account (like in the typical fluid approach). Such a matter corresponds to a charged dusty fluid, within the general astrophysical conception corresponding to a matter consisting of very tiny dust particles or multiple atomic-molecular clusters (see Sec. V for more details).

^{*}jiri.kovar@fpf.slu.cz

Circling around a compact object, under the influence of gravitational and electromagnetic actions of the central body and ambient fields, the considered charged fluid takes the toroidal-like form. As shown many times, for a purely neutral fluid [14–23], the effects of gravity are crucial for the toroidal configurations. However, we have shown that distribution of even small charges in the fluid interacting with an external electromagnetic field strongly influences its geometrical configuration, providing us with new interesting classes of toroidal topology.

Within the considered model, we have recently performed studies of the electrically charged perfect fluid encircling a charged black hole immersed into an asymptotically uniform magnetic field, imposing the assumption of rigid (constant angular velocity) rotation of the structures [24]. We focused on regular toroidal structures centered in the equatorial plane ($\theta = \pi/2$) and also on unique structures referred to as polar clouds located around polar axis ($\theta = 0$) of the black hole. Here, moreover, we pay attention to the third class of the structures. These are represented by the off-equatorial “levitating” tori, i.e. the tori centered in latitudes $0 < \theta < \pi/2$. As we have shown within our Newtonian studies [25], such structures can exist within a weak-field approximation, requiring, however, the gravitational field to be accompanied by a dipole magnetic field. Now, along with the equatorial tori, we reveal the existence and basic properties of the off-equatorial tori within the relativistic generalization; rotating with constant specific angular momentum and also in permanent rigid rotation, the tori are studied in a spherically symmetric gravitational field described by the Schwarzschild metric and pervaded with a test dipole magnetic field.

Our work is of theoretical scope essentially, being focused on a topological classification of the toroidal structures. However, for the purpose of a basic physical discussion we admit the standard, for decades accepted, astrophysical idealization. It is the concept of the fluid torus representing the equilibrium state of thick “accretion” discs that encircle a compact object, generating the assumed background fields (see Fig. 1). For a basic astrophysical contextualization, we can relate the compact object to an idealized magnetic neutron star. In general, investigation of charged particles motion in neutron stars magnetospheres ranks in attractive astrophysical applications of electromagneto-gravitodynamics; for instance, we can mention the classical works [26–29]. And, although the general formalism was developed long time ago, in the early 1970s, the subject has recently received a new impetus in the context of accretion disc coronae around compact stars and black holes in X-ray binaries. While the accretion takes place predominantly within the orbital plane of the binary system, diluted plasma occurs also outside the disc, where it forms a hot medium and a base of the jet near the symmetry axis. However, the exact mechanism of feeding this coronal region with charged particles, their transport

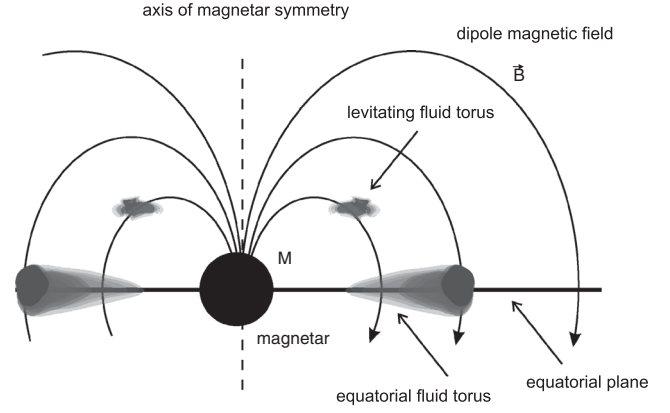


FIG. 1. Scheme of the considered situation—compact object endowed with dipole-type magnetic field accompanied by circling equatorial and off-equatorial “levitating” tori.

from the tenuous accretion disk, and acceleration in a collimated outflow remain as yet unknown. To this end, understanding the structure of the regions of stability is of great relevance.

Throughout the paper, we use the geometrical system of units [$\hat{c} = \hat{G} = \hat{k}_B = 1/(4\pi\hat{\epsilon}_0) = 1$] for quantities denoted by a bar, \bar{x} , thus expressed through units of length. These become dimensionless x when being scaled by the mass of the central black hole \bar{M} . For the direct interpretation, we express our results also in physical (SI) units denoted as \hat{x} .

II. MODEL OF CHARGED FLUID TORI

The presented investigation of charged fluid circling in strong gravitational and electromagnetic fields is based on fundamental magnetohydrodynamic equations, which, under particular assumptions determining our model, provide coupled partial differential pressure equations. After matching the thermodynamical quantities and introduction of an auxiliary function, these pressure equations, together with an integrability condition, allow us to find a rich family of topologically different classes of equipressure surfaces. These surfaces map possible shapes of equilibrium toroidal configurations of the studied fluid, being dependent on the chosen rotational law and on the so-called correction function (related to charge distribution), which must be selected from a class of functions determined through the integrability condition. Finally, the desired pressure (density, temperature and charge density) profiles can be easily expressed by means of the solution for the auxiliary function.

A. Simplifying assumptions and basic features

In our model, we generally assume fluid immersed in prescribed axially symmetric gravitational $g_{\alpha\beta}$ and electromagnetic $F_{\alpha\beta} = \nabla_\alpha A_\beta - \nabla_\beta A_\alpha$ fields, where, due to the symmetry, the vector potential has the form $A_\alpha = (A_t, A_\phi, 0, 0)$ in the coordinate system (t, ϕ, r, θ) . The axial

symmetry of the background represents the first simplifying assumption of the model, being physically very realistic. As the second simplifying assumption, we consider a test charge fluid only, i.e. nongravitating (rarefied) and slightly charged, thus without any contribution to the spacetime metric and the electromagnetic potential.

Within the magnetohydrodynamic approach, our conception of the charged fluid model is characterized by three basic features. Firstly, it is the zero electric conductivity of the fluid; secondly, it is the zero viscosity of the fluid. Such an idea represents a scenario of charges adherent to the moving single-component dielectric perfect fluid. The third basic feature of the model is that the fluid rotates in the purely ϕ -direction around the central compact object, i.e. with the 4-velocity $U^\alpha = (U^t, U^\phi, 0, 0)$, specific angular momentum $\ell = -U_\phi/U_t$ and angular velocity (with respect to distant observers) $\omega = U^\phi/U^t$; all related by the formulas

$$\omega = -\frac{\ell g_{tt} + g_{t\phi}}{\ell g_{t\phi} + g_{\phi\phi}}, \quad (1)$$

$$(U_t)^2 = \frac{g_{t\phi}^2 - g_{tt}g_{\phi\phi}}{\ell^2 g_{tt} + 2\ell g_{t\phi} + g_{\phi\phi}}. \quad (2)$$

Consequently, the 4-current density J^α of the fluid must have the only nonvanishing spatial component corresponding to the azimuthal flow of the charge density q_ρ ,

$$J^\phi = q_\rho U^\phi, \quad (3)$$

as it follows from the general expression of Ohm's law:

$$J^\alpha = q_\rho U^\alpha + \sigma F^{\alpha\beta} U_\beta. \quad (4)$$

Note that the zero conductivity $\sigma = 0$ of the fluid is a necessary condition for the self-consistency of the model. Really, if there was a nonzero conductivity $\sigma \neq 0$, the second term on the right-hand side of Ohm's law (4) would give rise to a radial electric current, unless there was a significant self-field, which is contradicting our assumption of self-fields omission. Thus, a radial electric current would imply the existence of a charge (electrons, ions) radial motion. This is, however, contradicting the basic feature of our model: the one requiring the azimuthal motion only since the charges are fixed (or directly forms) to moving matter.

B. Pressure equations

The rotating fluid with profiles of charge density q_ρ and energy density ϵ forms a torus determined by its iso-surfaces of the pressure p (equipressure surfaces), which can be determined from coupled "pressure" equations

$$\begin{aligned} \partial_r p &= -(p + \epsilon)\mathbb{R}_1 + q_\rho \mathbb{R}_2 \equiv \mathbb{R}, \\ \partial_\theta p &= -(p + \epsilon)\mathbb{T}_1 + q_\rho \mathbb{T}_2 \equiv \mathbb{T}, \end{aligned} \quad (5)$$

where $\mathbb{R} = \mathbb{R}(r, \theta)$ and $\mathbb{T} = \mathbb{T}(r, \theta)$ denote the right-hand sides of these equations, and

$$\mathbb{R}_1 = \partial_r \ln |U_t| - \frac{\omega \partial_r \ell}{1 - \omega \ell}, \quad (6)$$

$$\mathbb{R}_2 = U^t \partial_r A_t + U^\phi \partial_r A_\phi, \quad (7)$$

$$\mathbb{T}_1 = \partial_\theta \ln |U_t| - \frac{\omega \partial_\theta \ell}{1 - \omega \ell}, \quad (8)$$

$$\mathbb{T}_2 = U^t \partial_\theta A_t + U^\phi \partial_\theta A_\phi. \quad (9)$$

For better understanding, the pressure equations can be derived from the conservation laws and Maxwell's equations,

$$\nabla_\beta T^{\alpha\beta} = 0, \quad (10)$$

$$\nabla_\beta F^{\alpha\beta} = 4\pi J^\alpha, \quad (11)$$

$$\nabla_{(\gamma} F_{\alpha\beta)} = 0. \quad (12)$$

Here, the electromagnetic tensor $F^{\alpha\beta}$ describes the composition of the vacuum external electromagnetic field pervading the fluid, and the internal electromagnetic self-field of the fluid, i.e.

$$F^{\alpha\beta} = F_{\text{EXT}}^{\alpha\beta} + F_{\text{INT}}^{\alpha\beta}. \quad (13)$$

Similarly, the stress-energy tensor $T^{\alpha\beta}$ can be split into two parts: the matter and electromagnetic parts as

$$T^{\alpha\beta} = T_{\text{MAT}}^{\alpha\beta} + T_{\text{EM}}^{\alpha\beta}, \quad (14)$$

where

$$T_{\text{MAT}}^{\alpha\beta} = (\epsilon + p)U^\alpha U^\beta + p g^{\alpha\beta}, \quad (15)$$

$$T_{\text{EM}}^{\alpha\beta} = \frac{1}{4\pi} \left(F^\alpha{}_\gamma F^{\beta\gamma} - \frac{1}{4} F_{\gamma\delta} F^{\gamma\delta} g^{\alpha\beta} \right). \quad (16)$$

Assuming the stress-energy tensor decomposition (14) and appreciating that due to Maxwell's equations (11) and (12) we have [30]

$$\nabla_\beta T_{\text{EM}}^{\alpha\beta} = -F^{\alpha\beta} J_\beta, \quad (17)$$

we obtain the equation

$$\nabla_\beta T_{\text{MAT}}^{\alpha\beta} = F^{\alpha\beta} J_\beta, \quad (18)$$

following directly from the conservation laws (10).

The basic assumption of our model is to consider the test tori only, i.e. we have $F_{\text{INT}}^{\alpha\beta} \ll F_{\text{EXT}}^{\alpha\beta}$, and can put $F^{\alpha\beta} = F_{\text{EXT}}^{\alpha\beta}$. Then, the Eq. (18) implies the final “master” formula

$$\nabla_\beta T_{\text{MAT}}^{\alpha\beta} = F_{\text{EXT}}^{\alpha\beta} J_\beta. \quad (19)$$

Now, taking into account our first simplifying assumption (the background axial symmetry) and the third basic feature of the model (matter azimuthal circulation), we directly get the pressure equations (5).

C. Thermodynamical setup

Along with the considered simplifications and features characterizing the model (axial symmetry, negligible self-fields, zero conductivity and viscosity, and the pure azimuthal motion), we further introduce a couple of optional, but still very physical, simplifications. They allow us to clearly and relatively simply solve the pressure equations (5) in a pure analytical way. The first of such simplifications concerns adjustment of thermodynamical relations necessary for any further investigation.

In reality, intending to treat all the relevant phenomena, the thermodynamical description of accretion discs represents a very delicate problem. Especially, generation of heat and radiation makes the situation very complex. Here, for the purpose of a basic theoretical investigation, we restrict to low temperature adiabatic tori, i.e. we neglect the influence of radiation [31]. We consider a perfect fluid under an adiabatic polytropic relation

$$p = \kappa \rho^\Gamma, \quad (20)$$

with κ and Γ being polytropic coefficient and exponent, respectively, and ρ is the rest-mass density. Neglecting the radiation, especially the radiation pressure, we can assume that in the first approximation the pressure is of thermal nature only and determined by the ideal gas relation

$$p = \frac{1}{\langle m \rangle m_u} \rho T, \quad (21)$$

where m_u is the dimensionless atomic mass unit and $\langle m \rangle$ is the mean molecular weight [32]. For the following rough temperature estimations and discussions, we fix $\langle m \rangle \sim 1$, corresponding to simple atoms or molecules. In the considered case (no radiation), the energy density is given by the relation

$$\epsilon = \rho + \frac{1}{\Gamma - 1} p, \quad (22)$$

then we have $\epsilon = \epsilon(p)$.

Finally, note that in extreme astrophysical scenarios, we are often faced with the degenerated gas phase, with the pressure being temperature independent and related to the density only. In the case of ideal degenerate gas, we have the polytropic relation

$$p = \kappa_d \rho^\Gamma, \quad (23)$$

where κ_d is the polytropic coefficient of the degenerated matter.

D. Rotation and charge distribution

Looking at the pressure equations (5), we realize that they are not integrable, in general; the integrability condition

$$\partial_\theta \mathbb{R} + \mathbb{T} \partial_\rho \mathbb{R} = \partial_r \mathbb{T} + \mathbb{R} \partial_\rho \mathbb{T} \quad (24)$$

must be also satisfied. Regardless of this integrability condition, the existence of a solution of the pressure equations (5) is guaranteed for the zero charged density $q_\rho = 0$ only. This is when the last terms in equations (5) vanish, and we get the Euler equations describing a rotating electrically neutral (uncharged) perfect fluid [15,16].

In the case $q_\rho \neq 0$, the situation is more complicated since equations (5) are no longer integrable for arbitrary $q_\rho = q_\rho(r, \theta)$ and arbitrarily chosen $\ell = \ell(r, \theta)$. It is necessary to specify $\ell = \ell(r, \theta)$ (even with simplifications $\ell = \text{const}$ or $\omega = \text{const}$ being allowed) and find an appropriate distribution $q_\rho = q_\rho(r, \theta)$, which is consistent with that. Or, vice versa, we can specify $q_\rho = q_\rho(r, \theta)$ (with even $q_\rho = \text{const}$ being possible) and find an appropriate $\ell = \ell(r, \theta)$; the charged tori must clearly have distributions of charge and angular momentum satisfying the integrability condition (24). This is, however, strictly “necessary” only if the equation of state is prescribed. Otherwise, one could absorb this constraint into it.

E. Background description

The dipole magnetic field considered here is represented by the only nonvanishing azimuthal component of the vector potential [33]

$$A_\phi = -\frac{3}{8} \mathcal{M} f_0 \sin^2 \theta = \mathcal{M} \mathcal{A}_\phi, \quad (25)$$

where

$$f_0 = 2 + 2r + r^2 \ln(1 - 2/r); \quad (26)$$

for a better transparency, we distinguish its variable part \mathcal{A}_ϕ and the constant dipole magnetic moment \mathcal{M} given by the relation [34]

$$\mathcal{M} = \frac{4\mathcal{R}^{3/2}(\mathcal{R} - 2)^{1/2}}{6(\mathcal{R} - 1) + 3\mathcal{R}(\mathcal{R} - 2)\ln(1 - 2\mathcal{R}^{-1})}\mathcal{B}. \quad (27)$$

Here, \mathcal{B} is the magnetic field strength measured at the radius \mathcal{R} in the equatorial plane; for simplicity, but without a remarkable influence on the precision, we assume it to be sufficiently low to satisfy the test-field approximation, thus not contributing to the spacetime geometry. That is for its unique simplicity but still sufficient relevance considered with the metric of the Schwarzschild type,

$$ds^2 = -\left(1 - \frac{2}{r}\right)dt^2 + \left(1 - \frac{2}{r}\right)^{-1}dr^2 + r^2(d\theta^2 + \sin^2\theta d\phi^2). \quad (28)$$

F. Transformation of pressure equations and correction function

Having the thermodynamical relations $\epsilon = \epsilon(p)$ and $\rho = \rho(p)$ set, and the specific angular momentum profile chosen, we can now determine the charge density distribution from the integrability condition (24) and calculate the final pressure profile from the pressure equations (5).

To avoid a direct numerical integration, we can, however, transform the nonlinear pressure equations (5) to linear ones. For this purpose, it is convenient to define the function

$$K = \frac{q\rho}{\epsilon + p}, \quad (29)$$

which implies the system of equations

$$\begin{aligned} \partial_r p &= -(p + \epsilon)(\mathbb{R}_1 - K\mathbb{R}_2), \\ \partial_\theta p &= -(p + \epsilon)(\mathbb{T}_1 - K\mathbb{T}_2). \end{aligned} \quad (30)$$

We address the function K as the “correction” function, mathematically ensuring the integrability of Eqs. (30), physically determining the charge density distribution according to relation (29). Along with the setting parameters, such as ℓ or ω , \mathcal{M} , κ and Γ , the correction function represents another degree of freedom in the model, which we set *a priori*.

In our approach, we conveniently introduce the auxiliary function $h(r, \theta)$ satisfying coupled transformation equations

$$\begin{aligned} \partial_r h &= \frac{\partial_r p}{(p + \epsilon)}, \\ \partial_\theta h &= \frac{\partial_\theta p}{(p + \epsilon)}, \end{aligned} \quad (31)$$

in the united form written as $dh = \frac{dp}{(p + \epsilon)}$. Then, we get the final system of linear differential equations

$$\begin{aligned} \partial_r h &= -(\mathbb{R}_1 - K\mathbb{R}_2), \\ \partial_\theta h &= -(\mathbb{T}_1 - K\mathbb{T}_2), \end{aligned} \quad (32)$$

which is accompanied by the integrability condition

$$\partial_\theta(\mathbb{R}_1 - K\mathbb{R}_2) = \partial_r(\mathbb{T}_1 - K\mathbb{T}_2). \quad (33)$$

Under the assumption $\epsilon = \epsilon(p)$, guaranteed by the chosen thermodynamical setup (22), the transformation function can be explicitly expressed as

$$h = \int_0^h dh = \int_0^p \frac{dp}{p + \epsilon} = \ln\left(1 + \frac{\Gamma\kappa^{\frac{1}{\Gamma}}p^{\frac{\Gamma-1}{\Gamma}}}{\Gamma-1}\right). \quad (34)$$

In general, the auxiliary function $h(p)$ simplifies not only the integration of the pressure equation, but the whole following investigation as well. Starting with a topology of considered toroidal structures, it is fully determined through equipressure $p = \text{const}$ (or equienergy density $\epsilon = \text{const}$) surfaces; the outside surface (edge) of the torus corresponds to the zero surface $p = 0$, the center to the pressure maximum. However, as we can see from relation (34), for the physically relevant values $p > 0$, it follows that $h(p) > 0$, being monotonously increasing; moreover, there is $h(p) = 0$ for $p = 0$. Consequently, positions of maxima and zero surfaces of the pressure p correspond to positions of extrema and zero surfaces of the h -function. Thus, we equivalently manage with the investigation of the h -function for the topological survey. Proceeding to an investigation of physical characteristics, as we show in the following paragraph, profiles of the pressure, mass density, temperature, specific charge, etc. can be easily recovered from the h -function as well.

In the considered background with the only nonvanishing magnetic field component A_ϕ , reducing second parts of the pressure equations to

$$\mathbb{R}_2 = U^\phi \partial_r A_\phi, \quad (35)$$

$$\mathbb{T}_2 = U^\phi \partial_\theta A_\phi, \quad (36)$$

it is, moreover, very convenient to rescale the correction function as

$$\mathcal{K} = U^\phi K. \quad (37)$$

Then, our final system of differential equations (32) can be written in the form

$$\begin{aligned} \partial_r h &= -\left(\partial_r \ln|U_t| - \frac{\omega \partial_r \ell}{1 - \omega \ell} - \mathcal{M}\mathcal{K} \partial_r \mathcal{A}_\phi\right), \\ \partial_\theta h &= -\left(\partial_\theta \ln|U_t| - \frac{\omega \partial_\theta \ell}{1 - \omega \ell} - \mathcal{M}\mathcal{K} \partial_\theta \mathcal{A}_\phi\right), \end{aligned} \quad (38)$$

indicating a possible unification.

G. Existence conditions

Before proceeding to the full topological and physical survey, we can start with the discussion of the tori existence, despite having no solution of the pressure equations (5), or (30) and (32) at hand.

At first, note that since $g_{tt} < 0$ ($r > 2$ in the considered metric), the condition $\ell^2 g_{tt} + g_{\phi\phi} > 0$ must be satisfied, as we can see from relation (2). Since $\ell = -\omega g_{\phi\phi}/g_{tt}$, that can be rewritten in two equivalent forms

$$\ell^2 < \frac{r^3 \sin^2 \theta}{r-2} \equiv \ell_{\text{ph}}^2 \quad \text{or} \quad \omega^2 < \frac{r-2}{r^3 \sin^2 \theta} \equiv \omega_{\text{ph}}^2, \quad (39)$$

as a matter of fact, equivalent expressions of the natural condition for the azimuthal velocity of the circling matter

$$v^2 = -\frac{g_{\phi\phi}}{g_{tt}} \omega^2 = -\frac{g_{tt}}{g_{\phi\phi}} \ell^2 < 1. \quad (40)$$

The function $\ell_{\text{ph}}^2(r)$ plays the role of an effective potential governing the photon motion in the equatorial plane. The function ℓ_{ph}^2 has one local extremum (minimum) $\ell_{\text{ph},c}^2 = 27$ located at $r_{\text{ph},c} = 3$, corresponding to the circular photon orbit (see Fig. 3).

If we index the position of the torus center as (r_c, θ_c) , the necessary conditions for the torus (center) existence can be written within the considered transformation (34) in the form

$$\partial_r h|_{r=r_c, \theta=\theta_c} = 0, \quad \partial_\theta h|_{r=r_c, \theta=\theta_c} = 0, \quad (41)$$

or $\mathbb{R}|_{r=r_c, \theta=\theta_c} = 0, \mathbb{T}|_{r=r_c, \theta=\theta_c} = 0$, equivalently.

Clearly, the above conditions do not guarantee the existence of the desired local maximum of h . For this purpose, we have to construct the Hessian matrix

$$\mathcal{H} = \begin{pmatrix} \partial_{rr}^2 h & \partial_{r\theta}^2 h \\ \partial_{\theta r}^2 h & \partial_{\theta\theta}^2 h \end{pmatrix}, \quad (42)$$

whereas in the points of local maxima, conditions

$$\partial_{\theta\theta}^2 h|_{r=r_c, \theta=\theta_c} < 0, \quad \det \mathcal{H}|_{r=r_c, \theta=\theta_c} > 0 \quad (43)$$

must be fulfilled. Note that due to the background and tori symmetries, the mixed partial derivatives in the equatorial plane automatically vanish; the conditions for maxima in the equatorial plane reduce to

$$\partial_{rr}^2 h|_{r=r_c, \theta=\theta_c} < 0, \quad \partial_{\theta\theta}^2 h|_{r=r_c, \theta=\theta_c} < 0. \quad (44)$$

Along the positions of tori centers, we are also interested in the so-called cusps of the tori. They correspond to the saddle points in the pressure (h -function) profiles, and the necessary conditions (41) must be satisfied for them as well.

H. Physical characteristics profiles

Having the polytropic equation of state (20) and the correction function (37) chosen, the pressure $p(r, \theta)$, mass density $\rho(r, \theta)$, temperature $T(r, \theta)$ and specific (per unit mass) charge $q(r, \theta)$ profiles of the tori can be determined through the h -function (34) as

$$p = \left(\frac{e^h - 1}{\kappa^{1/\Gamma}} \frac{\Gamma - 1}{\Gamma} \right)^{\frac{\Gamma}{\Gamma-1}}, \quad (45)$$

$$\rho = \left(\frac{p}{\kappa} \right)^{\frac{1}{\Gamma}} = \left(\frac{e^h - 1}{\kappa} \frac{\Gamma - 1}{\Gamma} \right)^{\frac{1}{\Gamma-1}}, \quad (46)$$

$$T = m_u \frac{p}{\rho} = m_u (e^h - 1) \frac{\Gamma - 1}{\Gamma}, \quad (47)$$

$$q = \frac{q_\rho}{\rho} = \frac{\mathcal{K}}{U^\phi} \left(\frac{\epsilon + p}{\rho} \right) = \frac{\mathcal{K}}{U^\phi} e^h. \quad (48)$$

For completeness, we note that unlike the considered fluid with ideal gas features, for the degenerate gas limit, the temperature assignment (47) loses its reliability completely; the other relations from the set remain valid for $\kappa = \kappa_d$.

Along with the physical limitation on the profiles (45)–(48) discussed later, we must be aware of the simplifying assumption in the model—the test tori requirements. For this purpose, we must check mass and charge of the torus, determined by the volume integrals

$$\mathfrak{M} = \int_{\mathcal{V}} \rho d\mathcal{V}, \quad \mathfrak{Q} = \int_{\mathcal{V}} q_\rho d\mathcal{V}; \quad (49)$$

in the case of the torus centered in the equatorial plane, we have

$$\mathfrak{M} = 4\pi \int_{r_{\text{in}}}^{r_{\text{out}}} \int_{\theta_{\rho_0}}^{\frac{\pi}{2}} \rho \sqrt{-g} d\theta dr, \quad (50)$$

$$\mathfrak{Q} = 4\pi \int_{r_{\text{in}}}^{r_{\text{out}}} \int_{\theta_{\rho_0}}^{\frac{\pi}{2}} q \rho \sqrt{-g} d\theta dr, \quad (51)$$

where r_{in} and r_{out} denote positions of the inner and outer edges of the structures in the equatorial plane, and θ_{ρ_0} is the function determining the upper half of the cross section of the outside surface of the torus with the poloidal plane

$(r \times \theta)$, given numerically from the equation $\rho = 0$; $g = -r^4 \sin^2 \theta$ is the determinant of the metric tensor reflected in the line element (28).

To compare the strength of the ambient dominant magnetic field with the one generated by the charged rotating torus, we can roughly estimate order of its strength close to edge of the torus by the following simplification. Assuming a torus, resembling the ideal mathematical regular torus with its cross-section radius $(r_{\text{out}} - r_{\text{in}})/2$, and “shrinking” it figuratively to the infinitely thin charged ring at the torus center $r = r_c$, we can estimate the order of the generated magnetic field strength as

$$\hat{\mathfrak{B}} \sim \frac{4\pi 10^{-7} \hat{I}}{2\pi(\hat{r}_{\text{out}} - \hat{r}_c)}, \quad (52)$$

in the distance $r_{\text{out}} - r_c$ from this center. Here, the constant $4\pi 10^{-7}$ represents the vacuum permeability in SI units, and $\hat{I} \sim \hat{\mathfrak{Q}}\hat{\omega}/(2\pi)$ is the estimation of the order of the total current through the cross section of the original torus.

I. Unique h -solution

The transformed pressure equations (38), following directly from Eqs. (32), provide a general system of equations for the unknown function $h(r, \theta)$. This can be determined from the system if the rotational law and charge distribution are chosen through the functions $\ell(r, \theta)$ and $\mathcal{K}(r, \theta)$ satisfying the integrability condition (33).

Under the assumptions $\omega = \omega(\ell)$ and $\mathcal{K} = \mathcal{K}(\mathcal{A}_\phi)$ (restricting degrees of freedom in the model, but still providing realistic physical scenarios), however, we can join the system of Eqs. (38) into the integral form

$$\int_0^h dh = -\ln \left| \frac{U_t}{U_{t_{\text{in}}}} \right| + \int_{\ell_{\text{in}}}^{\ell} \frac{\omega d\ell}{1 - \omega\ell} + \mathcal{M} \int_{\mathcal{A}_{\phi_{\text{in}}}}^{\mathcal{A}_\phi} \mathcal{K} d\mathcal{A}_\phi, \quad (53)$$

with the solution briefly written as

$$h = -H + H_{\text{in}}. \quad (54)$$

Here, after integration, the function $-H(r, \theta)$ represents the variable part in the right-hand side of Eq. (53), and the subscript “in” refers to the inner edge of the torus at $r = r_{\text{in}}$, $\theta = \theta_{\text{in}}$, determining the joined constants of integration H_{in} .

The united integral form of the pressure equations (53) is extremely convenient, allowing us to avoid a standard general treatment of coupled partial differential equations. As we show in the following paragraph, its noncharged limit is very useful for investigation of the neutral fluid [35].

J. “Polish doughnut” limit

Polish doughnuts represent electrically neutral perfect-fluid polytropic toroidal structures circling close to compact objects, originally constructed around Schwarzschild and Kerr black holes, and reflecting the corner stone contributions of the Polish school in their name [15,16]. In our model, we get such tori in the nonelectromagnetic limiting cases $q \rightarrow 0$ ($\mathcal{K} \rightarrow 0$), or $\mathcal{M} \rightarrow 0$. Then, in the case $\epsilon = \epsilon(p)$, the pressure profiles can be determined from the behavior of the uncharged limit of the auxiliary function h (54), here denoted as \tilde{h} and satisfying equations

$$\begin{aligned} \partial_r \tilde{h} &= -\left(\partial_r \ln |U_t| - \frac{\omega \partial_r \ell}{1 - \omega\ell} \right), \\ \partial_\theta \tilde{h} &= -\left(\partial_\theta \ln |U_t| - \frac{\omega \partial_\theta \ell}{1 - \omega\ell} \right); \end{aligned} \quad (55)$$

under the additional assumptions $\omega = \omega(\ell)$, we can also conveniently use the integral form of these equations, i.e. the formula

$$\int_0^{\tilde{h}} d\tilde{h} = -\ln \left| \frac{U_t}{U_{t_{\text{in}}}} \right| + \int_{\ell_{\text{in}}}^{\ell} \frac{\omega d\ell}{1 - \omega\ell} \equiv -\tilde{H} + \tilde{H}_{\text{in}}. \quad (56)$$

After the substitution $\tilde{h} = \int_0^p \frac{dp}{p+\epsilon}$, formula (56) is referred to as Boyer’s condition [16].

K. Magnetic field lines and equations projection

Considering more general scenarios of behavior of charged matter in combined gravitational and electromagnetic fields, an integration of the generalized form of pressure equations (5) represents a delicate problem. There is, however, a very useful technique based on integration along magnetic field lines, simplifying the study in many respects. An application of this method is nicely introduced in the work [29], where a similar problem of charged matter motion is treated in dipole magnetosphere of neutron star.

The magnetic field lines can be well represented by the tangent magnetic vector field B^a . For the considered dipole magnetic field, the only nonvanishing covariant local tetrad components are

$$B_{(r)} = F_{(\phi\theta)}, \quad B_{(\theta)} = -F_{(\phi r)}, \quad (57)$$

and being transformed to the Schwarzschild coordinates they read

$$B_r = \frac{e_{(\phi)}^\phi e_{(\theta)}^\theta}{e_{(r)}^r} F_{\phi\theta}, \quad B_\theta = -\frac{e_{(\phi)}^\phi e_{(r)}^r}{e_{(\theta)}^\theta} F_{\phi r}, \quad (58)$$

where $e_{(r)}^r = g_{rr}^{-1/2}$, $e_{(\phi)}^\phi = g_{\phi\phi}^{-1/2}$ and $e_{(\theta)}^\theta = g_{\theta\theta}^{-1/2}$ are the nonvanishing components of the tetrad basis vectors $e_{(r)}^\alpha$, $e_{(\phi)}^\alpha$ and $e_{(\theta)}^\alpha$. Thanks to the expression $F_{\alpha\beta} = \nabla_\alpha A_\beta - \nabla_\beta A_\alpha$, in the considered Schwarzschild metric $g_{\alpha\beta}$ and with the only nonvanishing vector potential component A_ϕ , we get the contravariant vector field components

$$B^r = -\frac{1}{(g_{rr}g_{\phi\phi}g_{\theta\theta})^{1/2}}\partial_\theta A_\phi, \quad (59)$$

$$B^\theta = \frac{1}{(g_{rr}g_{\phi\phi}g_{\theta\theta})^{1/2}}\partial_r A_\phi. \quad (60)$$

The pressure equations from the set (5) represent components of the vector equation $P_\alpha = 0$, where for the electromagnetic potential $A_\alpha = (0, A_\phi, 0, 0)$ there is

$$P_\alpha = \partial_\alpha p + (p + \epsilon)\left(\partial_\alpha \ln |U_t| - \frac{\omega \partial_\alpha \ell}{1 - \omega \ell}\right) - q_\rho U^\phi \partial_\alpha A_\phi. \quad (61)$$

Equation (61) can be projected (by scalar product with the magnetic vector field B^α) into the direction of the magnetic field lines $B^\alpha = (0, 0, B^r, B^\theta)$, providing us with the single equation $P_\alpha B^\alpha = 0$, or in explicit form

$$\frac{dp}{p + \epsilon} + d \ln |U_t| - \frac{\omega d\ell}{1 - \omega \ell} = 0, \quad (62)$$

where we used the relation $dr/d\theta = B^r/B^\theta$ valid (only) along magnetic field lines. In the special case $\ell = \text{const}$, and for the chosen thermodynamical setup with the polytropic equation of state, we get

$$h + \ln |U_t| = \text{const} \quad (63)$$

along magnetic field lines.

The consequence of the particular result (63) is that, except for constants, we obtain profiles of the h -function (pressure, density) along magnetic field lines without integration of the pressure equations. From another point of view, having the profiles of the h -function as the direct solution of the pressure equations (32), relation (63) immediately reveals the structure of magnetic field lines, independently of the type of the solution h parametrized by the rotational law and charge profile (see Fig. 2). Moreover, note that without the presence of the magnetic field (or the charge of the matter), relation (63) gives directly the general solution of the pressure equations, as can be checked after comparison with the solution of Eq. (56) [37].

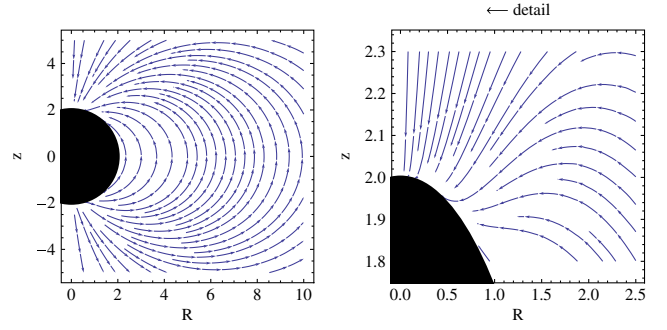


FIG. 2. Magnetic field lines of the considered dipole magnetic field. The lines are determined by the vector field B^α and conveniently plotted in cylindrical coordinates $R = r \sin \theta$ and $z = r \cos \theta$ above the event horizon.

III. TOPOLOGY OF ℓ AND ω CONSTANT TORI

In this section, we systematically go through a variety of topologically different toroidal configurations rotating in two different ways: with constant ℓ and constant ω [38]. The geometry of such tori is fully determined by the profiles of the function $h(r, \theta)$, depending on two parameters only: rotational parameter ℓ^2 or ω^2 and the electromagnetic parameter μ introduced later on. For an illustrative insight, however, we map the toroidal topology by means of equipotential surfaces of the potential $H(r, \theta)$, directly defined by the function h (54) and conveniently presented in the cylindrical coordinates $R = r \sin \theta$ and $z = r \cos \theta$.

Further, we also reveal that in the case of $\ell = \text{const}$ tori, the toroidal structures circling in the considered background exist in their uncharged limit in the equatorial plane and in both the charged equatorial and off-equatorial regimes. On the other hand, $\omega = \text{const}$ toroidal structures do not exist neither in the uncharged limit nor in the charged off-equatorial regime. The only possible $\omega = \text{const}$ configurations is the charged one settled in the equatorial plane.

A. Correction function specification

No matter which distribution of specific angular momentum we choose ($\ell = \text{const}$ or $\omega = \text{const}$), the integrability condition (33) can be rewritten in the form

$$4 \cos \theta \partial_r \mathcal{K} - f_1 (r \cos \theta \partial_r \mathcal{K} - \sin \theta \partial_\theta \mathcal{K}) = 0, \quad (64)$$

where

$$f_1 = -2 + 2r + (r - 2)r \ln(1 - 2/r), \quad (65)$$

in the case $0 < \theta < \pi$ having the analytical solution

$$\mathcal{K} = \mathcal{K}(r, \theta) = \mathcal{K}(\sqrt{-f_0} \sin \theta). \quad (66)$$

The correction function $\mathcal{K}(r, \theta)$ is a generic function which must be chosen. And, as we can see from a comparison of relations (66) and (25), it must fit the class of arbitrary functions with the only argument \mathcal{A}_ϕ , i.e. $\mathcal{K}(r, \theta) = \mathcal{K}(\mathcal{A}_\phi)$. Such a dependence is not an optional specific need for the simplification of the pressure equations, which can be then written in the united form (53). It is the most general integrability requirement in the considered background and rotational regimes; Eq. (53) provides fully equivalent solutions to those following from the system of Eqs. (38).

In the studied cases $\ell = \text{const}$ and $\omega = \text{const}$, we choose the generic function in two exemplary forms

$$\mathcal{K} = k\mathcal{A}_\phi, \quad (67)$$

$$\mathcal{K} = k\mathcal{A}_\phi^3, \quad (68)$$

respectively, where k is a constant. Rewriting relations (67) and (68) by using relations (29) and (37), we find

$$q_\rho = k \frac{\mathcal{A}_\phi(p + \epsilon)}{U^\phi}, \quad (69)$$

$$q_\rho = k \frac{\mathcal{A}_\phi^3(p + \epsilon)}{U^\phi}, \quad (70)$$

respectively. Thus, it turns out that k plays the role of a charge scaling factor. In more details, it is a quantity allowing us to specify “how much” charged our matter is. Together with the magnetic moment \mathcal{M} , it represents the free parameter in the model.

B. Electromagnetic parameter and sign convention

In the pressure equations (38) for the h -function, the charged scaling parameter k occurs in the product with the magnetic moment \mathcal{M} only. Therefore, we can introduce the coupled electromagnetic parameter (effective magnetic moment)

$$\mu = k\mathcal{M}, \quad (71)$$

playing an important role in the next discussions.

Referring to relations (69) and (70), we can interpret sign of μ in the following way. Considering the orientation of the dipole magnetic moment (dipole magnetic field) to be fixed as $\mathcal{M} > 0$ (oriented along the symmetry axis z), then the sign of the electromagnetic parameter μ is the same as the sign of the charge parameter k . Thus, positive values $\mu > 0$ mean the positive (counterclockwise) rotation $U^\phi > 0$ ($\ell > 0$ and $\omega > 0$) of the positively charge matter $q_\rho > 0$, or the negative (clockwise) rotation $U^\phi < 0$

($\ell < 0$ and $\omega < 0$) of the negatively charge matter $q_\rho < 0$. On the other hand, negative values $\mu < 0$ mean the positive rotation $U^\phi > 0$ of the negatively charge matter $q_\rho < 0$ or the negative rotation $U^\phi < 0$ of the positively charge matter $q_\rho > 0$.

C. Equatorial $\ell = \text{const}$ neutral tori

In order to well understand the relatively complex situation with the charged tori characterized by a rich classification of different configurations, and for the purpose of comparison and emphasis of the electromagnetic interaction in our model, we briefly recover the $\ell = \text{const}$ configurations in their uncharged (Polish doughnut) limit.

The second of necessary conditions (41) implies that the neutral $\ell = \text{const}$ tori are allowed only in the equatorial plane ($\theta_c = \pi/2$); the first one implies for the locations of the torus center r_c (and cusp) the relation

$$\ell^2 = \tilde{\ell}_c^2(r_c) \equiv \frac{r_c^3}{(r_c - 2)^2}. \quad (72)$$

According to the first of sufficient conditions (44), we find that the center of the torus exists for $r_c > 6$ only.

Trying to interpret the uncharged limit of the h -function, we easily reveal its energy nature. In the $\ell = \text{const}$ case, there is

$$\begin{aligned} \tilde{h} &= -\tilde{H} + \tilde{H}_{\text{in}} = -\ln|U_t| + \ln|U_{t_{\text{in}}}| \\ &= -\ln \tilde{E} + \ln \tilde{E}_{\text{in}}, \end{aligned} \quad (73)$$

where $\tilde{E} = -U_t$ is the specific (per unit mass) energy of particles moving along circular geodesics with specific angular momentum $\tilde{L} = U_\phi$. The function $\tilde{H} = \ln \tilde{E}$ then plays the role of a potential. It fully represents the character of the \tilde{h} -function behavior since \tilde{H}_{in} is only the constant of integration, having its physical meaning only for setting the edge (size) of the torus in the prescribed \tilde{H} -potential field [39].

The extrema of \tilde{H} (as well as the extrema of \tilde{h}) are located in the equatorial plane only. For their localization, we can conveniently map behavior of the equatorial profile of the potential \tilde{H} , i.e. the one-dimensional potential $\tilde{H}_{\pi/2}(r) \equiv \tilde{H}(r, \theta = \pi/2)$, having its extrema determined by the function $\tilde{\ell}_c^2$ (72) shown in Fig. 3. The function $\tilde{\ell}_c^2$ embodies one local minimum $\tilde{\ell}_{\text{ms}} = 27/2$ corresponding to the squared specific angular momentum of particles moving along the marginally stable circular orbit at $r = 6$. The radii determined from the condition $\ell^2 = \tilde{\ell}_c^2(r_c)$ correspond to unstable (smaller radius) and stable (greater radius) circular geodesics. The stable one determines the position of the torus center, where the potential \tilde{H} and its equatorial profile $\tilde{H}_{\pi/2}$ have local minimum, while

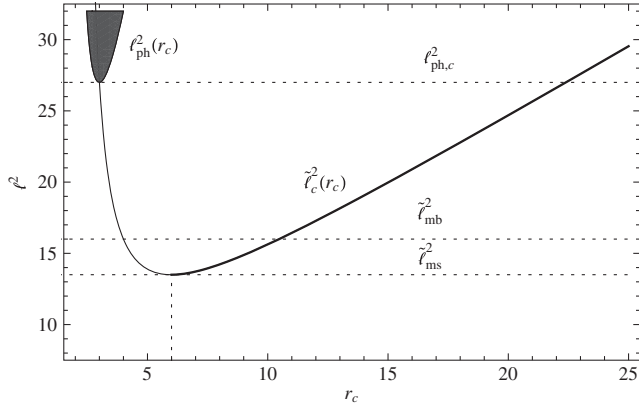


FIG. 3. Behavior of the function $\tilde{\ell}_c^2(r_c)$ governing extrema of the potential $\tilde{H}(r, \theta)$ in the equatorial plane. For a fixed value of the squared angular momentum ℓ^2 , we can clearly determine positions of the potential maximum (smaller radius) and minimum (larger radius) as the intersections of $\tilde{\ell}_c^2(r_c)$ curve and $\ell^2 = \text{const}$ line. The potential $\tilde{H}(r, \theta)$ is not defined in the black region limited by the function $\ell_{ph}^2(r_c)$. The toroidal structures with $\ell^2 = \text{const}$ exist only for $\ell^2 > \tilde{\ell}_{ms}^2$.

the \tilde{h} -function and the corresponding pressure p are maximal there. The unstable geodesic determines a critical point (cusp), where the potential \tilde{H} has the saddle point, and $\tilde{H}_{\pi/2}$ has a local maximum there.

Clearly, the toroidal configurations can exist only for $\ell^2 > \tilde{\ell}_{ms}^2$, when both the extrema (minimum and maximum) of $\tilde{H}_{\pi/2}$ are present. For $\ell^2 > \ell_{ph,c}^2$, only the local minimum is present since we are limited by the condition $\ell^2 < \ell_{ph}^2$ (39) represented by the forbidden-black region in Fig. 3. In addition to the limits $\ell_{ph,c}^2$ and $\tilde{\ell}_{ms}^2$, there is one more characteristic value $\tilde{\ell}_{mb}^2 = 16$. It corresponds to the square of specific angular momentum of particles moving along the marginally bound equatorial circular geodesic at $r = 4$. The toroidal structures with $\ell^2 < \tilde{\ell}_{mb}^2$ can form a cusp.

Mapping behavior of the \tilde{H} -potential through its equipotential surfaces, we can emphasize the so-called “critical surface,” which is the self-crossing surface corresponding to the maximum (cusp) of $\tilde{H}_{\pi/2}$ (saddle point of \tilde{H}) and the “null” $\tilde{H} = 0$ equipotential surface crossing the equatorial plane at infinity. The behavior of the potential \tilde{H} can be summarized in the following ways:

For $\ell^2 \in (0, \tilde{\ell}_{ms}^2)$, there are no extrema of the potential \tilde{H} , no closed equipotential surfaces and no critical equipotential surface (see Fig. 4A).

For $\ell^2 = \tilde{\ell}_{ms}^2$, there is one inflexion point of the potential \tilde{H} in the equatorial plane. There, the critical surface has its critical point corresponding to a ring. The null equipotential surface is open towards the black hole (see Fig. 4B).

For $\ell^2 \in (\tilde{\ell}_{ms}^2, \tilde{\ell}_{mb}^2)$, there is a negative saddle point and a negative local minimum of the potential \tilde{H} in the equatorial plane (negative maximum and negative minimum of $\tilde{H}_{\pi/2}$). In this case, closed equipotential surfaces exist. They are bounded by the critical surface self-crossing in the cusp located between r_{ms} and r_{mb} . The null equipotential surface is open towards the black hole (see Fig. 4C).

For $\ell^2 = \tilde{\ell}_{mb}^2$, there is a zero saddle point and a negative minimum of the potential \tilde{H} in the equatorial plane (zero maximum and negative minimum of $\tilde{H}_{\pi/2}$). The closed equipotential surfaces are bounded by the critical surface which coincides with the null equipotential surface (see Fig. 4D).

For $\ell^2 \in (\tilde{\ell}_{mb}^2, \ell_{ph,c}^2)$, there is a positive saddle point and a negative minimum of the potential \tilde{H} in the equatorial plane (positive maximum and negative minimum of $\tilde{H}_{\pi/2}$). The closed equipotential surfaces are bounded by the outer null equipotential surface. The critical surface is now open outwards away from the black hole and self-crosses between the radii $r_{ph,c}$ and r_{mb} (see Fig. 4E).

For $\ell^2 = \ell_{ph,c}^2$, the potential \tilde{H} diverges at $r_{ph,c}$ and the saddle point no longer exists. The negative local minimum of the potential \tilde{H} is still present. The closed equipotential surfaces are bounded by the outer null equipotential surface. The critical surface is no longer present.

For $\ell^2 > \ell_{ph,c}^2$, the only extremum of the potential \tilde{H} is the negative minimum. The closed equipotential surfaces are bounded by the outer null equipotential surface. There is no longer any critical surface, but there is a forbidden region for fluid elements with prescribed specific angular momentum, delimited by the radii satisfying the relation $\ell^2 = \ell_{ph}^2(r_c)$ (see Fig. 4F).

D. Equatorial $\ell = \text{const}$ charged tori

Since the second from the necessary conditions (41) is automatically satisfied in the equatorial plane, the centers and cusps of the $\ell = \text{const}$ torus in the equatorial plane can be determined through the first of them; the choice of the correction function in the form (67) implies the relation

$$\ell^2 = \ell_c^2(r_c; \mu) \equiv \frac{r^3(4 + 3\mu r \mathcal{A}_\phi f_1)}{(r-2)(4r-8 + 3r\mu \mathcal{A}_\phi f_1)} \Big|_{r=r_c}. \quad (74)$$

In dependence on the effective moment μ , the sufficient conditions (44) then reveal the tori existence region in the parametric plane $(r_c \times \ell^2)$ as shown in Fig. 5.

In contrast to the neutral tori, there are three different types A, B, C of behavior of the function $\ell_c^2(r_c; \mu)$ determining the stationary points of the potential H for the negative values of μ , and three types D, E and F for the positive ones (see Fig. 5). Extrema of the function ℓ_c^2 are determined from the condition $\partial_r \ell_c^2 = 0$, implicitly defining functions $\mu_{\ell, \text{ex} \pm}(r_c)$ taking their local extrema

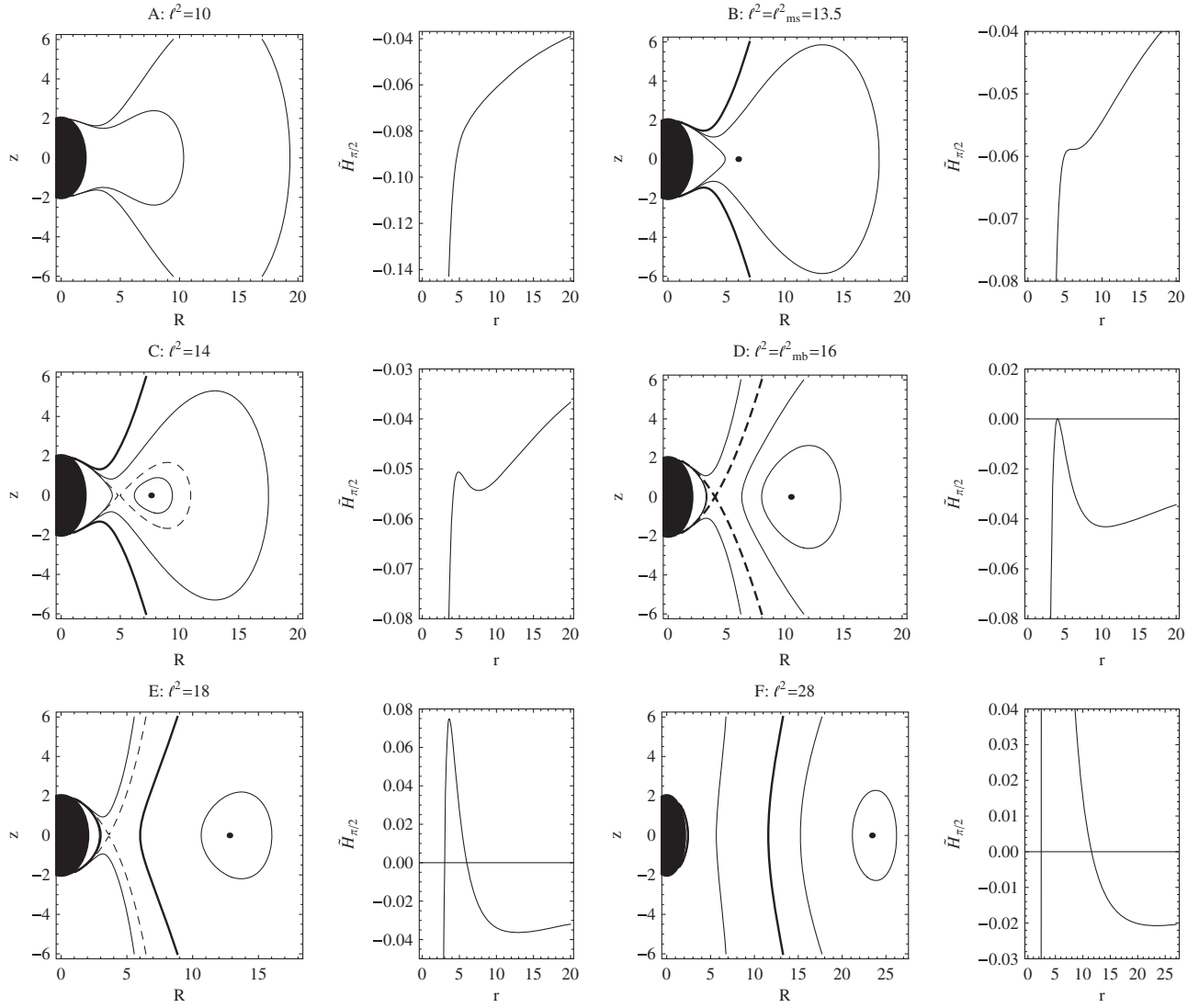


FIG. 4. Typical behavior of the potential $\tilde{H}(r, \theta)$ shown in terms of its equipotential surfaces and equatorial profile $\tilde{H}_{\pi/2}$. Taking progressively increasing values of the squared specific angular momentum ℓ^2 , we present six qualitatively different types of behavior of the potential. The dashed and thick curves correspond to critical and null equipotential surfaces, respectively; the dots denote locations of minima and inflexion point of the potential \tilde{H} .

$\mu_{AB} \doteq -0.37$, $\mu_{BC} \doteq -0.33$, $\mu_{DE} \doteq 2.4$ and $\mu_{EF} \doteq 3.0$. We find that for:

$\mu \in (-\infty, \mu_{AB})$, the function ℓ_c^2 has one minimum on the upper branch of its behavior (type A);

$\mu \in (\mu_{AB}, \mu_{BC})$, the function ℓ_c^2 has minimum on each of its branches and one maximum on its lower branch (type B);

$\mu \in (\mu_{BC}, 0)$, the function ℓ_c^2 has one minimum on its right branch (type C);

$\mu \in (0, \mu_{DE})$, the function ℓ_c^2 has one minimum on its single branch (type D);

$\mu \in (\mu_{DE}, \mu_{EF})$, the function ℓ_c^2 has two minima and one maximum on its single branch (type E). This class can be also separated into two subclasses $\mathbb{E}1$ and $\mathbb{E}2$ according to the comparison of the values of both the minima;

$\mu \in (\mu_{EF}, \infty)$, the function ℓ_c^2 has one minimum on its single branch (type F).

Each from the types of the function $\ell_c^2(r_c; \mu)$ provides several different classes of behavior of the potential H , which full classification is outside the scope of this paper. We, however, present two very interesting cases of the H -potential topology: those related to the B and E types of the function ℓ_c^2 behavior (see Fig. 6).

E. Off-equatorial $\ell = \text{const}$ charged tori

According to the necessary conditions (41), the $\ell = \text{const}$ off-equatorial tori can be centered in the positions determined through relations

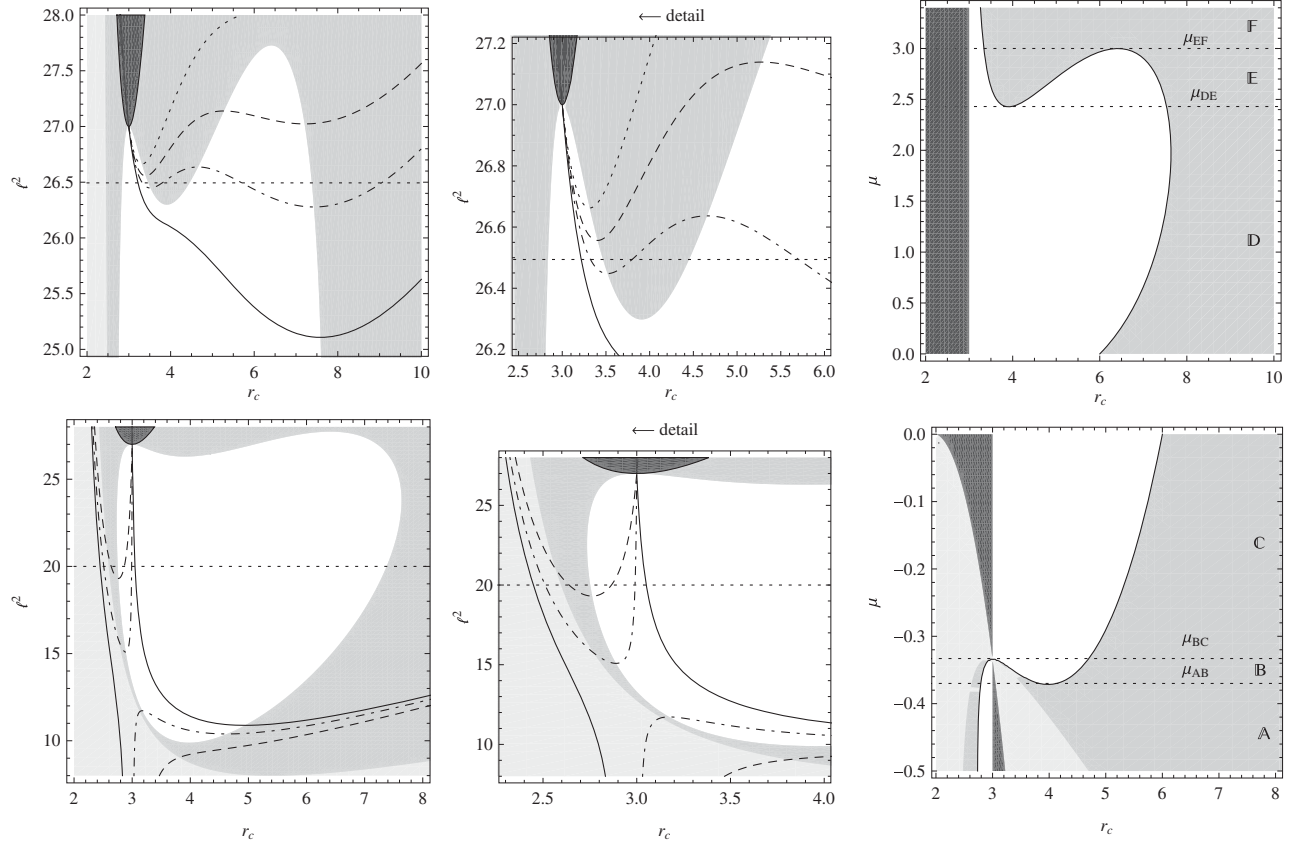


FIG. 5. Profiles of the function $\ell_c^2(r_c; \mu)$ governing extrema of the potential $H(r, \theta)$ in the equatorial plane (first two plots in row), and profiles of the functions $\mu_{\ell, \text{ex}\pm}(r_c)$ (thick) determining extrema of $\ell_c^2(r_c; \mu)$ (last plot in row). For $\mu < 0$ (lower row), we can find three different types of behavior of the function ℓ_c^2 , particularly $\ell_{cA}^2(r_c; -0.4)$ (dashed), $\ell_{cB}^2(r_c; -0.34)$ (dot-dashed) and $\ell_{cC}^2(r_c; -0.3)$ (solid) in dependence on values of the parameter μ chosen from intervals A, B and C determined by extrema of the function $\mu_{\ell, \text{ex}-}(r_c)$. For $\mu > 0$ (upper row), we can also find three different types of behavior of the function ℓ_c^2 , particularly $\ell_{cD}^2(r_c; 2.3)$ (solid), $\ell_{cE1}^2(r_c; 2.6)$ (dot-dashed) or $\ell_{cE2}^2(r_c; 2.8)$ (dashed), and $\ell_{cF}^2(r_c; 3.1)$ (dotted) in dependence on values of the parameter μ chosen from intervals D, E and F determined by extrema of the function $\mu_{\ell, \text{ex}+}(r)$. Reading the figure, for a fixed value of ℓ^2 , we can clearly determine positions of the H -potential extrema in the equatorial plane as the intersections of a particular $\ell_c^2(r_c; \mu)$ curve and $\ell^2 = \text{const}$ line. Intersections located in the light-gray region correspond to minima in the r -direction only. The full local minima are related to the intersections from the dark-gray region. The intersections in the white region correspond to maxima in the r -direction. Especially, see the intersections of the dotted lines $\ell^2 \doteq 26.5$ and $\ell^2 = 20$ with the $\ell_{cE1}^2(r_c; 2.6)$ and $\ell_{cA}^2(r_c; -0.4)$ curves, corresponding to the positions of extrema of the potential H plotted in Fig. 6. For completeness, note that the potential H is not defined in the black region limited by the function $\ell_{\text{ph}}^2(r_c)$.

$$\ell^2 = -\frac{r^3 f_0 \sin^2 \theta}{4(r-2)} \Big|_{\substack{r=r_c \\ \theta=\theta_c}}, \quad (75)$$

$$\mu = -\frac{4}{3 \sin^2 \theta (f_0 + 4) \mathcal{A}_\phi} \Big|_{\substack{r=r_c \\ \theta=\theta_c}}. \quad (76)$$

Following relation (40), we find for the azimuthal velocity of the torus center the limitation

$$v_c^2 \equiv 1 - \frac{1}{4} f_0|_{r=r_c} < 1. \quad (77)$$

Equivalently, we have $v_c^2 - 1 = -\frac{f_0+4}{4} < 0$ or $f_0 + 4 > 0$ for $r = r_c$, which requires the torus center location at

positions $r_c \geq 2.3231$ independently on the latitude θ_c . We also find that the first of sufficient conditions (43) is automatically satisfied; the second one, however, provides us with the final restriction $r_c \geq 4.1817$ independently on θ_c .

Further investigation of the H -potential configurations incorporating the off-equatorial minima requires discussion in the four-dimensional parametric space ($r \times \theta \times \ell^2 \times \mu$). In contrast to the discussions of the equatorial configurations, having one degree of freedom ($\theta = \pi/2$) less, here, we manage with the pure statement of the existence and limitation. Again, we do not go through the full discussion. Instead, we present the typical two-lobe H -potential topology containing separated off-equatorial lobes formed around their centers (potential minima) and those joined

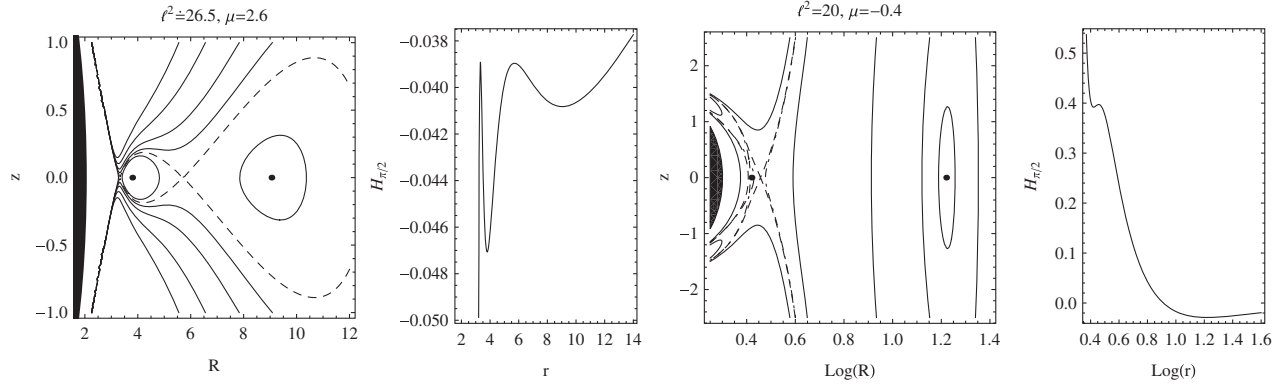


FIG. 6. Typical behavior of the potential $H(r, \theta)$ shown in terms of its equipotential surfaces and equatorial profiles $H_{\pi/2}(r)$. Particularly, we present the topology determined by the parameters $\ell^2 \doteq 26.5$ and $\mu = 2.6$ (left part), embodying two minima and two saddle points in the equatorial plane; all of them determined by the function $\ell_{cE1}^2(r; 2.6)$. There is also the topology determined by the parameters $\ell^2 = 20$ and $\mu = -0.4$ (right part). This is characteristic for its two minima and one saddle point in the equatorial plane determined by the function $\ell_{cA}^2(r; -0.4)$ and two saddle off-equatorial points (for an insight into the area around the saddle points see Fig. 7). The dashed curves correspond to critical equipotential surfaces self-crossing in the equatorial saddle points. The dot-dashed curves correspond to critical equipotential surfaces self-crossing in the off-equatorial saddle points. The thick dots denote the locations of potential minima.

through a throat in the equatorial plane (area of the potential saddle point) (see Fig. 8).

F. Absence of equatorial $\omega = \text{const}$ neutral tori

Beginning the survey of the $\omega = \text{const}$ tori, we start with a comment on their uncharged limit. The necessary conditions (41) restrict possible centers of such tori into the equatorial plane and to the radii related to the angular velocity as

$$\tilde{\omega}^2 = \tilde{\omega}_c^2(r_c) \equiv \frac{1}{r_c^3}. \quad (78)$$

First of the sufficient conditions (44), however, demands for the tori centers $r_c < 3$, which contradicts the condition (39). In general, independently of the rotational law, in the case of a purely azimuthal motion of the neutral fluid, its center corresponding to a circular geodesic must be located at radii $r > 3$, i.e. above the photon circular orbit. Thus, the

$\omega = \text{const}$ tori do not exist until they are electrically charged, as we show in the next paragraph.

G. Equatorial $\omega = \text{const}$ charged tori

By charging the $\omega = \text{const}$ rotating torus, from conditions (41) and for the chosen correction function (68), we find that the tori centers and cusps are automatically allowed in the equatorial plane at positions given by the relation

$$\omega^2 = \omega_c^2(r_c; \mu) \equiv \frac{(r-2)(4+3r\mu A_\phi^3 f_1)}{r^3(4r-8+3r\mu A_\phi^3 f_1)} \Big|_{r=r_c}. \quad (79)$$

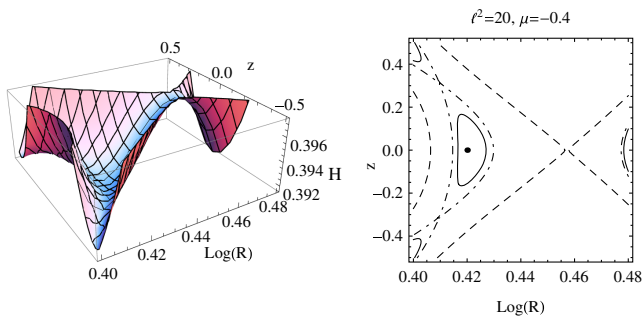


FIG. 7. Behavior of the potential $H(r, \theta)$ determined by the parameters $\ell^2 = 20$ and $\mu = -0.4$ close to its saddle points (for more details see Fig. 6).

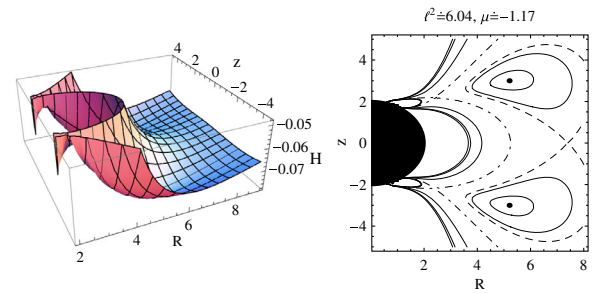


FIG. 8. Typical behavior of the potential $H(r, \theta)$ shown in terms of its full profile and equipotential surfaces. The presented topology is determined by the parameters $\ell^2 \doteq 6.04$ and $\mu = -1.17$ and embodies separated off-equatorial lobe structures around the potential minima and also those joined through a saddle point in the equatorial plane. The dashed curves correspond to critical equipotential surfaces self-crossing in the equatorial saddle points. The dot-dashed curves correspond to critical equipotential surfaces self-crossing in the off-equatorial saddle points. The thick dots denote the locations of potential minima.

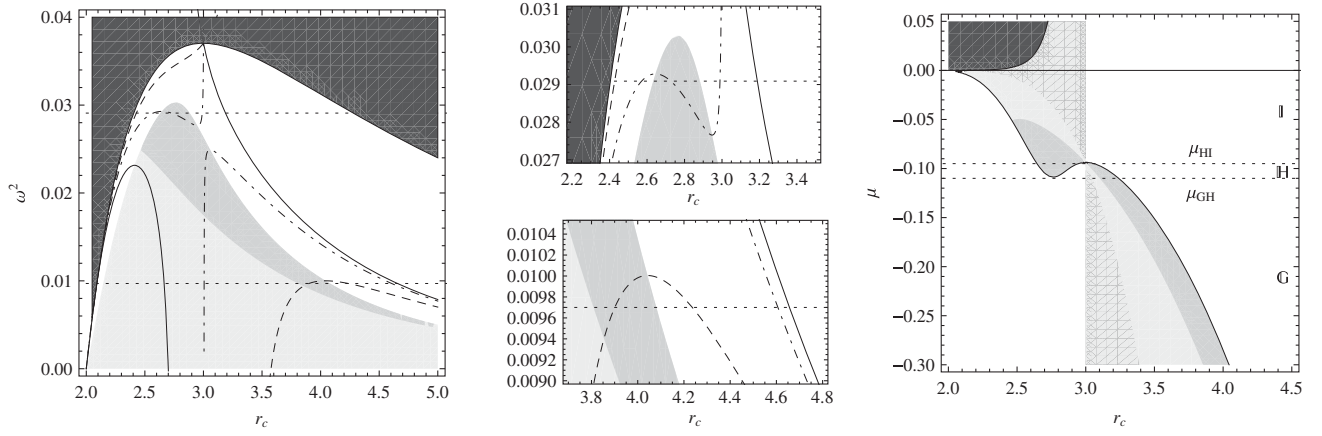


FIG. 9. Profiles of the function $\omega_c^2(r_c; \mu)$ governing extrema of the potential $H(r, \theta)$ in the equatorial plane (first two plots in row) and profiles of the function $\mu_{\omega, \text{ex}}(r_c)$ (thick) determining extrema of $\omega_c^2(r_c; \mu)$ (last plot in row). For $\mu < 0$, we can find three different types of behavior of the function ω_c^2 , particularly $\omega_{cG}^2(r_c; -0.3)$ (dashed), $\omega_{cH}^2(r_c; -0.095)$ (dot-dashed) and $\omega_{cI}^2(r_c; -0.04)$ (solid) in dependence on values of the parameter μ chosen from intervals \mathbb{G} , \mathbb{H} and \mathbb{I} determined by the extrema of the function $\mu_{\omega, \text{ex}}(r_c)$. For $\mu > 0$ we cannot find minima of the potential H . Reading the figure, for a fixed value of the squared angular velocity ω^2 , we can clearly determine positions of the H -potential extrema in the equatorial plane as the intersections of a particular $\omega_c^2(r)$ curve and $\omega^2 = \text{const}$ line. Intersections located in the light-gray region correspond to minima in the r -direction only. The full local minima are related to the intersections from the dark-gray region. The intersections in the white region correspond to maxima in the r -direction. Especially, see the intersections of the dotted lines $\omega^2 \doteq 0.02909$ and $\omega^2 = 0.0097$ with the $\omega_{cH}^2(r_c; -0.095)$ and $\omega_{cG}^2(r_c; -0.3)$ curves, corresponding to the positions of extrema of the potential H plotted in Fig. 10. For completeness, note that the potential H is not defined in the black region limited by the function $\omega_{\text{ph}}^2(r_c)$.

In dependence of the electromagnetic parameter μ , the sufficient conditions (44) imply the tori center existence in the region of the parametric plane $(r_c \times \omega^2)$ as shown in Fig. 9.

Going through the classification in the similar manner as in Sec. III D, we find three different types \mathbb{G} , \mathbb{H} and \mathbb{I} of behavior of the function $\omega_c^2(r_c; \mu)$ determining the stationary points of the potential H for the negative

values of μ . For positive values, there are no minima of the potential H , i.e. no toroidal structures, as demonstrated in Fig. 9. Extrema of the function ω_c^2 are determined from the condition $\partial_r \omega_c^2 = 0$, implicitly defining the function $\mu_{\omega, \text{ex}}(r_c)$ taking its extrema $\mu_{GH} \doteq -0.110$ and $\mu_{HI} \doteq -0.094$. We find that for: $\mu \in (-\infty, \mu_{GH})$, the function ω_c^2 has one maximum on its right branch (type \mathbb{G});

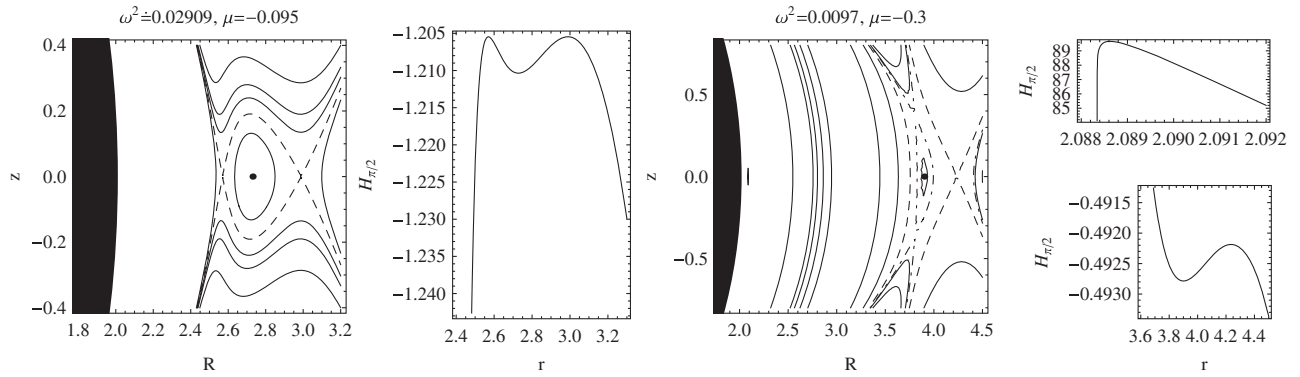


FIG. 10. Typical behavior of the potential $H(r, \theta)$ shown in terms of its equipotential surfaces and equatorial profile $H_{\pi/2}(r)$. Particularly, we present the topology determined by the parameters $\omega^2 \doteq 0.02909$ and $\mu = -0.095$ (left part), embodying one minimum and two saddle points in the equatorial plane, all of them determined by the function $\omega_{cH}^2(r_c; -0.095)$. There is also the topology determined by the parameters $\omega^2 = 0.0097$ and $\mu = -0.3$ (right part). This is characteristic for its one local minimum, one saddle point and one maximum in the equatorial plane determined by the function $\omega_{cG}^2(r_c; -0.3)$ and for its two off-equatorial saddle points (for an insight into the area around the maximum see Fig. 11). The dashed curves correspond to critical equipotential surfaces self-crossing in the equatorial saddle points. The dot-dashed curves correspond to critical equipotential surfaces self-crossing in the off-equatorial saddle points. The thick dots denote locations of potential minima.

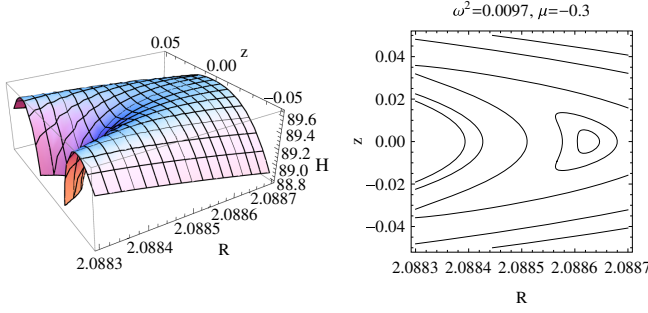


FIG. 11. Behavior of the potential $H(r, \theta)$ determined by the parameters $\omega^2 = 0.0097$ and $\mu = -0.3$ close to its maximum (for more details see Fig. 10).

$\mu \in (\mu_{\text{GH}}, \mu_{\text{HI}})$, the function ω_c^2 has maximum on each of its branches and one local minimum on its left branch (type \mathbb{H});

$\mu \in (\mu_{\text{HI}}, 0)$, the function ω_c^2 has one maximum on its left branch (type \mathbb{I}).

Each from the types of the function $\omega_c^2(r_c; \mu)$ provides several different classes of behavior of the potential H , together revealing a rich classification of them, as well as in the $\ell = \text{const}$ case. Also here, we skip this classification and present two interesting cases of the H -potential topology, those related to the \mathbb{G} and \mathbb{H} types of the function ω_c^2 behavior in Fig. 10.

H. Absence of off-equatorial $\omega = \text{const}$ charged tori

In contrast to the $\ell = \text{const}$ tori, the rigidly rotating $\omega = \text{const}$ tori cannot be formed above the equatorial plane for any choice of the correction function $\mathcal{K} = \mathcal{K}(\mathcal{A}_\phi)$.

That is because the necessary conditions (41) imply the stationary points of the h -function satisfying the relations

$$\omega^2 = -\frac{(r-2)f_0}{4r^3 \sin^2 \theta} \Big|_{\substack{r=r_c \\ \theta=\theta_c}}, \quad (80)$$

$$\mathcal{M} = -\frac{4}{3 \sin^2 \theta (f_0 + 4) \mathcal{K}} \Big|_{\substack{r=r_c \\ \theta=\theta_c}}, \quad (81)$$

and for the azimuthal velocity of the torus center we find the same limitation (77) as in the case of off-equatorial $\ell = \text{const}$ tori. Thus, we require $f_0 + 4 > 0$ and $f_0 < 0$ for $r = r_c$, which demands the torus center location at positions $r_c > 2.3231$ independently on θ_c .

Under these assumptions the sufficient conditions (43) can be rewritten in the form

$$\sin^2 \theta (f_0 + 4) \frac{\partial \mathcal{A}_\phi \mathcal{K}}{\mathcal{K}} \Big|_{\substack{r=r_c \\ \theta=\theta_c}} > \frac{8}{3}, \quad (82)$$

$$\sin^2 \theta (f_0 + 4) \frac{\partial \mathcal{A}_\phi \mathcal{K}}{\mathcal{K}} \Big|_{\substack{r=r_c \\ \theta=\theta_c}} < \frac{8}{3} \frac{f_2}{f_0 f_3} \Big|_{\substack{r=r_c \\ \theta=\theta_c}}, \quad (83)$$

where

$$f_2 = 4(r^3 + r^2 + 5r + 9) + 4r^2(r^2 + 2) \ln \left(1 - \frac{2}{r}\right) + r^4(r-1) \left[\ln \left(1 - \frac{2}{r}\right) \right]^2, \quad (84)$$

$$f_3 = 3r^2 + r^2(r-1) \ln \left(1 - \frac{2}{r}\right) + 6. \quad (85)$$

Since $\frac{f_2}{f_0 f_3} < 1$ for $r_c > 2.3231$, conditions (82) and (83) are contradicting; thus, the rigidly rotating off-equatorial tori cannot exist in the considered background.

IV. PROCEDURE OF TORUS CONSTRUCTION

The previous Sec. III was focused on the geometrical investigation of topologically different toroidal configurations. Studying different types of the two-parametric (μ, ℓ) or (μ, ω) h -function solution (54), we introduced the main part of the presented work. However, for a basic contextualization, we gladly enhance the paper with an elementary physical discussion of the tori properties based on relations (45)–(48). Constructing theoretically relevant tori, along with the limitations given by the assumptions of the model, we must be also aware of the most fundamental astrophysical restrictions on the tori and background. Following the scheme of the fluid toroidal structures imitating the equilibrium state of accretion discs, we can roughly estimate how much “close” or “far” from this idealization the constructed tori could be.

A. Torus limitations

Trying to list the physical restriction on the fluid forming an equilibrium configuration representing an accretion disc, one can be surprised by an enormous number of them. Within the scope of this paper, we manage with the idea of nondegenerated matter not being subjected to the nuclear reaction. For this purpose, we roughly compare and restrict the extrema of the pressure, density and temperature profiles of the constructed tori below the solar core values $\hat{p}_\odot \sim 10^{16}$ Pa, $\hat{\rho}_\odot \sim 10^5$ kg m⁻³ and $\hat{T}_\odot \sim 10^7$ K representing our upper limits.

The temperature must be kept certainly low not only to prevent the matter from nuclear reactions. In our model, we neglect the torus radiation pressure $\sim T^4$. Thus, within the consistency, the temperature should be as low as possible in the precise and severe verdict.

Similarly, the density must be kept low not only due to nuclear reactions. Clearly, the dense fluid forms heavy

torus and also leads to its high total charge. Such generates strong magnetic field comparable with the ambient one, violating the simplifying assumption of the test torus. Of course, both the low mass and small charge requirements can be met even for highly dense tori, but such tori have to be relatively tiny and slightly charged. In this respect, we can ask, how much rarefied matter we can afford. This is clearly limited by the considered magnetohydrodynamic approach. Usually, the upper limit for the kinetic approach applicability (rarefied fluids) is the number density up to 10^{24} m^{-3} . Considering particles of approximately proton mass $\hat{m}_p \sim 10^{-27} \text{ kg}$, we get the mass density limit $\hat{\rho}_{\text{MHD}} \gtrsim 10^{-3} \text{ kg m}^{-3}$.

Within the specific charge profile setting, we must be aware of the high specific charge of the order of $q_p \sim 10^{18}$, representing the specific charge for elementary proton-like particles (cations). For the purpose of minimization of the total charge of the torus, however, the specific charge should be kept lower in orders.

B. Torus construction and two-parameter tuning

In the wide range of parameters (μ, ℓ or ω, Γ, κ and H_{in}) entering the geometrical and physical characteristics of the tori, the construction of the physically relevant tori (tori with reasonable profiles of pressure p , density ρ , temperature T , specific charge q , etc.) might have seemed not clear enough. We can, however, choose a well-arranged method providing us with an efficient procedure of the tori construction and profiles modification.

At first, we must realize that the geometry of the torus, studied through the investigation of the h -function solution in previous section, also directly determines profiles of the physical characteristics given by relations (45)–(48). Geometry is, however, not the only factor for the physical setup. That is also the torus matter origin. Thus, we can look at the construction of the torus from two interfering points of view. These are (i) choice of the geometric characteristics (fully determined through the h -function) and (ii) determination of the matter parameters Γ and κ (yielding reasonable profiles of the physical characteristic together with the chosen h -function).

We start with determination of the geometry (type and size) of the torus determined through the h -function. The structure of the h -solution reads $h = -H + H_{\text{in}}$, where the potential H prescribe the type (shape, and positions of centers and cusps) of the torus. The potential H is uniquely determined by two parameters: the electromagnetic (field-matter) parameter μ and the torus rotational law (parameters ℓ or ω). The integration constant H_{in} shifts values of the potential up and down only, setting this way the edge of the torus (zero surface), i.e. the size of the torus.

Next step is to choose the matter parameters Γ and κ . Being focused on the nonrelativistic matter approximation, we can put the polytropic exponent $\Gamma = 5/3$. Any change within the physically realistic values $1 < \Gamma < 2$, however,

does not influence the characteristics profiles dramatically; thus, the only parameter, which should be chosen carefully, is the polytropic coefficient κ .

We can see that having the type of the torus set (μ, ℓ (or ω)), we still have two degrees of freedom due to two parameters: the geometric (size) parameter H_{in} and the matter parameter κ . Proper balancing of them yields the feasible physical characteristics. In more details, the effective construction of the torus can be realized in the following steps:

- (1) Choice of the torus type (shape, positions of centers and cusps) through the parameters μ, ℓ (or ω). This also implicitly sets the profiles of all the physical characteristics, which will be tuned in the following steps.
- (2) Choice of the torus size through the parameter H_{in} . This primarily sets the temperature profile, however, it also simultaneously sets the pressure and density profiles, which will be finally tuned in the last step.
- (3) Choice of the fluid type through the parameter κ . This tunes the final pressure and density profiles, and does not touch the previous κ independent temperature profile.
- (4) Check of the total charge of the torus and generated magnetic field. If the total charge is high enough to generate the magnetic field comparable with the ambient magnetic field, we must either decrease the size of the torus through the parameter H_{in} or the density profile through the parameter κ (the specific charge profile itself is κ independent). Of course, there is also the option to entirely change the type of the torus by changing parameters μ, ℓ (or ω); as a matter of fact, this means to start with point (1) again.

C. Exemplary toroidal structures

In this paragraph, we present several samples of tori with the geometry determined by the previously presented profiles of the H -potential. We choose values of the geometric parameter H_{in} and matter parameters κ and Γ , so that they match (or illustratively mismatch) the above mentioned physical limits. In all the presented cases, we exemplary set the parameters to be $\kappa = 10^6$ and $\Gamma = 5/3$, whereas the geometric constant H_{in} varies in the samples. Moreover, we choose the mass of the central compact object to be $\hat{M} = \hat{M}_{\odot}$ and define its radius $\mathcal{R} = 3$, under which all the profiles lose their meaning. The magnetic field strength is set to $\mathcal{B} \doteq 4.24 \times 10^{-8}$ (in SI units corresponding to the value $\hat{\mathcal{B}} = 10^8 \text{ T}$) in the equatorial plane at the compact object surface $r = \mathcal{R}$. This choice corresponds to the dipole moment of the magnetic field $\mathcal{M} \doteq 4.2 \times 10^{-7}$. Such a kind of the central object setup follows from the considered idealization of the object imitating a magnetic star, as we comment below in more details. Note that the assumed

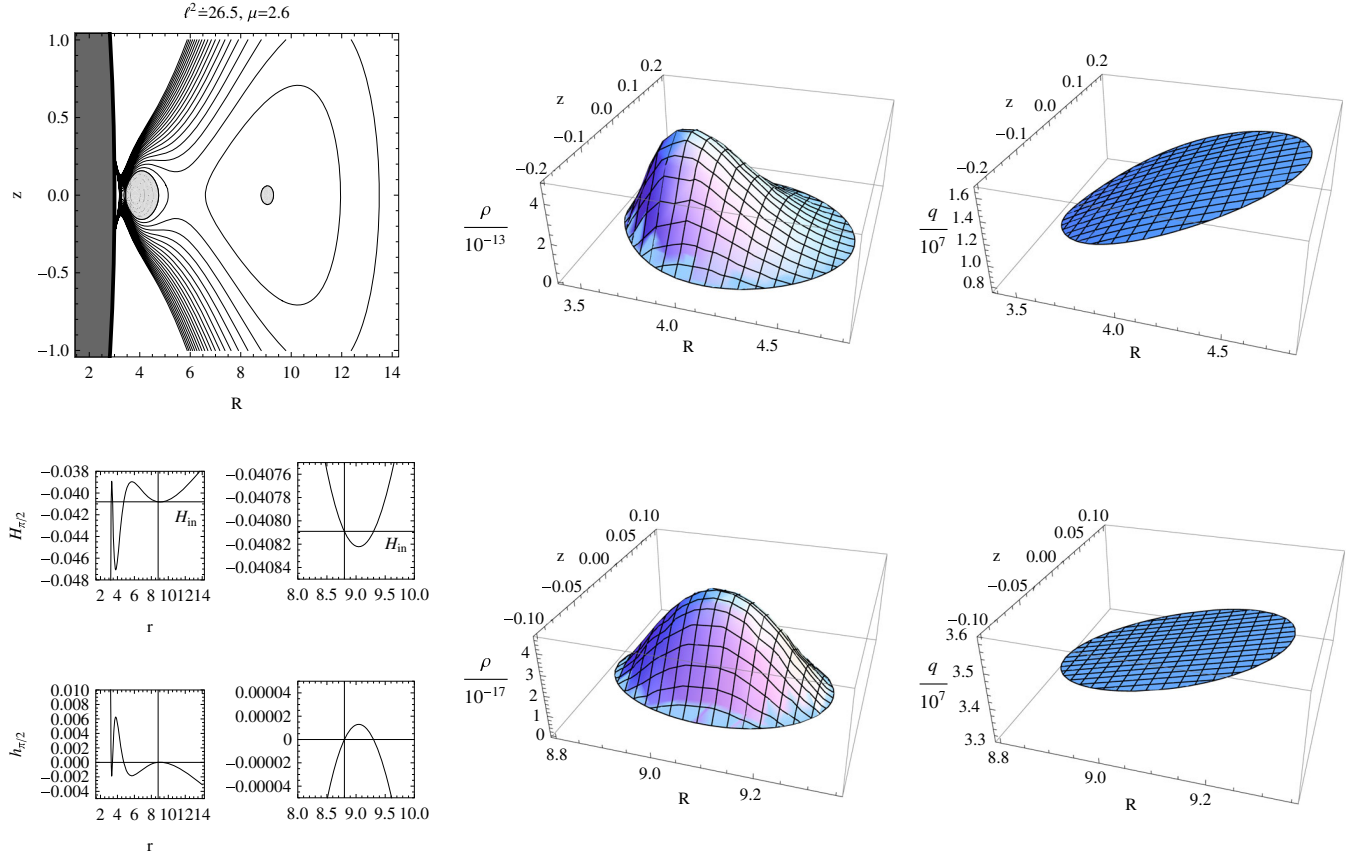


FIG. 12. Positively charged equatorial $\ell^2 \doteq 26.5$ tori counterclockwise rotating in the field with the electromagnetic parameter $\mu = 2.6$. Along with the equipotential H surfaces, we plot equatorial profiles of the potential H and the related h -function. The three-dimensional plots map the density ρ and specific charge q profiles corresponding to the parameters $H_{\text{in}} \doteq -0.041$, $\kappa = 10^6$ and $\Gamma = 5/3$.

magnetic field strength is consistent with our test-field assumption; even the magnetic fields $\hat{B} \sim 10^{11}$ T can be considered as the test fields [4].

1. $\ell = \text{const}$ equatorial tori

The presented $\ell = \text{const}$ equatorial tori (see Fig. 12) are assigned to the behavior of the H -potential determined by the parameters $\ell^2 \doteq 26.5$ and $\mu = 2.6$ (see Fig. 6), embodying two minima at $r_c \doteq 3.8$ and $r_c \doteq 9.1$ and two saddle points in the equatorial plane. In dependence on the value of the parameter H_{in} , such a topology allows construction of one or two separated tori with the centers corresponding to the minima of the potential H or two tori joint through the cusp. Here, we show a sample of two separated tori, determined by the value $H_{\text{in}} \doteq -0.041$ corresponding to the inner edges of the tori at $r_{\text{in}} \doteq 3.4$ (larger torus) and $r_{\text{in}} = 8.8$ (smaller torus) in the equatorial plane.

The central pressure, density and temperature of the inner (greater) torus reach in dimensionless units their maxima $p_c \sim 10^{-15}$, $\rho_c \sim 10^{-13}$ or in physical SI units $\hat{p}_c \sim 10^{23}$ Pa, $\hat{\rho}_c \sim 10^8$ kg m $^{-3}$, $\hat{T}_c \sim 10^{10}$ K. The total

charge of the torus reaches $\mathfrak{Q} \sim 10^{-5}$, and the generated dipole magnetic field from the torus (close to its surface) can be estimated as $\mathfrak{B} \sim 10^{-6}$. We can see that the inner torus does not fit all the considered limits described above, and, moreover, neither does our assumption of the test torus since we have $\mathfrak{B} \gg \mathcal{B}$ here.

The central pressure, density and temperature of the outer (smaller) torus reach their maxima $p_c \sim 10^{-23}$, $\rho_c \sim 10^{-17}$ or equivalently $\hat{p}_c \sim 10^{16}$ Pa, $\hat{\rho}_c \sim 10^4$ kg m $^{-3}$, $\hat{T}_c \sim 10^8$ K. The total charge of the torus and the generated dipole magnetic field are $\mathfrak{Q} \sim 10^{-9}$ and $\mathfrak{B} \sim 10^{-10}$, respectively. This torus fits our limits, except for the slightly higher temperature; our assumption of the test torus is fulfilled.

2. $\ell = \text{const}$ off-equatorial tori

The presented $\ell = \text{const}$ off-equatorial tori (see Fig. 13) are assigned to the behavior of the H -potential determined by the parameters $\ell^2 \doteq 6.042$ and $\mu \doteq -1.167$ (see Fig. 8), embodying two minima (surrounded by two topological lobes) at the radius $r_c = 6$, and latitudes $\theta_c = \pi/3$ and $\theta_c = 2\pi/3$, two saddle points

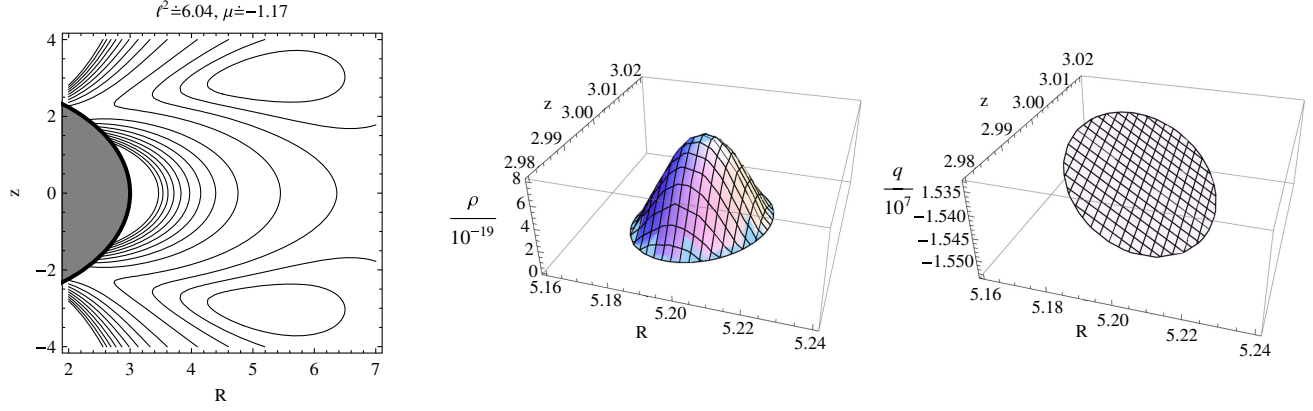


FIG. 13. Negatively charged off-equatorial $\ell^2 \doteq 6.042$ tori counterclockwise rotating in the field with the electromagnetic parameter $\mu \doteq -1.167$. The three-dimensional plots map the density ρ and specific charge q profiles corresponding to the parameters $H_{\text{in}} \doteq -0.0781$, $\kappa = 10^6$ and $\Gamma = 5/3$.

outside the equatorial plane and one saddle point (lobes connection) in the equatorial plane. In dependence on the value of the parameter H_{in} , such a topology allows construction of two separated off-equatorial tori with the centers corresponding to the local minima of the potential or the construction of the off-equatorial tori joint through the cusp in the equatorial plane. Here, we chose $H_{\text{in}} \doteq -0.0781$, determined by the choice of the torus edge at $r_{\text{in}} = 5.98$ and $\theta_{\text{in}} = \pi/3$ or $\theta_{\text{in}} = 2\pi/3$, and get two separated rather small tori.

The central pressure, density and temperature of the tori reach their maxima $p_c \sim 10^{-24}$, $\rho_c \sim 10^{-18}$ or equivalently $\hat{p}_c \sim 10^{13}$ Pa, $\hat{\rho}_c \sim 10^2$ kg m $^{-3}$, $\hat{T}_c \sim 10^7$ K. The total charge of each torus and the generated dipole magnetic field are $\mathfrak{Q} \sim -10^{-13}$ and $\mathfrak{B} \sim -10^{-14}$, respectively. Thus, these off-equatorial tori meet all our limitations as well as the assumption of the test tori, though they have to be really small.

3. $\omega = \text{const}$ equatorial tori

The presented $\omega = \text{const}$ equatorial torus (see Fig. 14) is assigned to the behavior of the H -potential determined by the parameters $\omega^2 = 0.0097$ and $\mu = -0.3$ (see Fig. 10), embodying one minimum at $r_c = 3.9$ and one saddle point in the equatorial plane. The choice of the parameter $H_{\text{in}} \doteq -0.493$, determined by the choice of the position of the inner edge $r_{\text{in}} = 3.892$ in the equatorial plane, leads to the simple bounded torus here.

The central pressure, density and temperature of the torus presented in Fig. 14 reach their maxima $p_c \sim 10^{-24}$, $\rho_c \sim 10^{-18}$ or equivalently $\hat{p}_c \sim 10^{14}$ Pa, $\hat{\rho}_c \sim 10^3$ kg m $^{-3}$, $\hat{T}_c \sim 5 \times 10^7$ K. The total charge of the torus and the generated dipole magnetic field are $\mathfrak{Q} \sim -10^{-13}$ and $\mathfrak{B} \sim -10^{-13}$, respectively. Also here, this sample torus meets all our limitations as well as the assumption of the test torus.

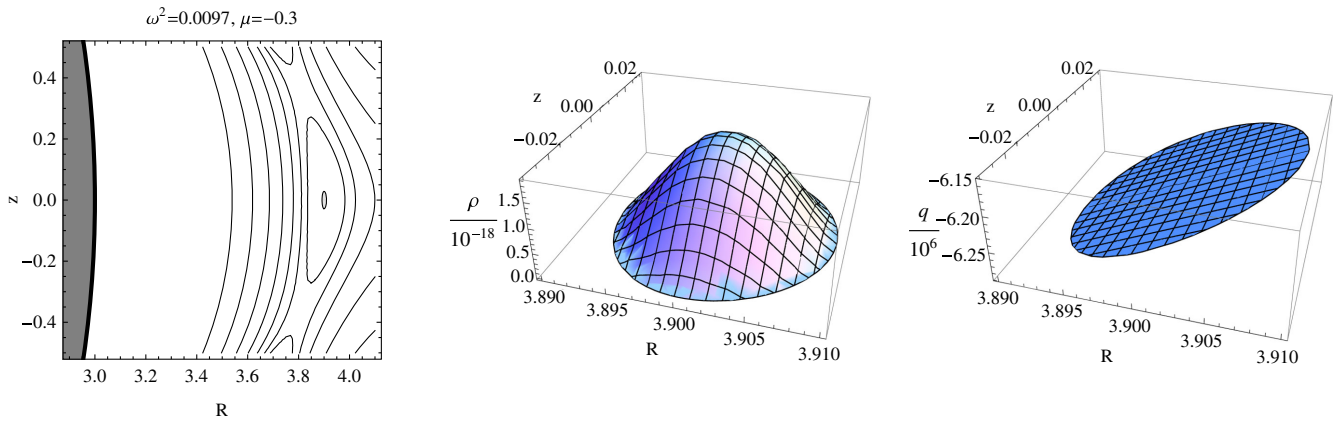


FIG. 14. Negatively charged equatorial $\omega^2 = 0.0097$ torus counterclockwise rotating in the field with the electromagnetic parameter $\mu = -0.3$. The three-dimensional plots map the density ρ and specific charge q profiles corresponding to the parameters $H_{\text{in}} \doteq -0.493$, $\kappa = 10^6$ and $\Gamma = 5/3$.

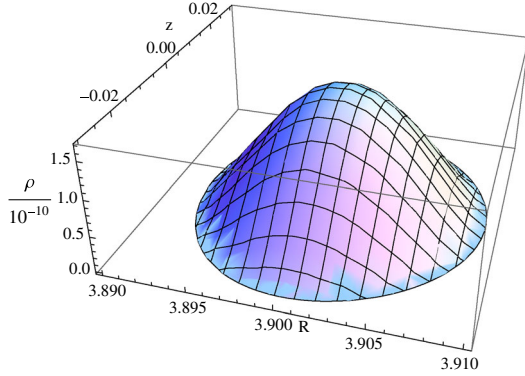


FIG. 15. Density profile of negatively charged equatorial $\omega^2 = 0.0097$ torus counterclockwise rotating in the field with the electromagnetic parameter $\mu = -0.3$ shown in Fig. 14 and differing in the value of the polytropic parameter only, here being fixed to $\kappa = \kappa_{\text{dn}} \doteq 5$.

On the other hand, for a comparison, the torus presented in Fig. 15 reaches extremely high values of the density $\rho_c \sim 10^{-10}$. They were achieved by the change of the polytropic parameter to $\kappa = \kappa_{\text{dn}} \doteq 5$ or equivalently $\hat{\kappa} = (3\pi^2)^{2/3} \hat{\hbar}^2 / (5\hat{m}_n^{8/3}) \doteq 5 \times 10^3 \text{ Pa kg}^{-5/3} \text{ m}^5$, with the rest parameters being kept; the parameter κ_{dn} corresponds to the polytropic parameter of the ideal degenerated neutron gas. As a direct consequence of the extreme density, the total charge of the torus reaches $\mathfrak{Q} \sim -10^{-5}$ and generates the magnetic field $\mathfrak{B} \sim -10^{-5}$, exceeding the ambient field by orders and thus violating the assumption of test field.

V. DISCUSSION

A. Background idealization—Magnetic star

It is well known that the application of Schwarzschild geometry is typical for investigation of processes in static and spherically symmetric gravitational fields of Schwarzschild black holes. There is, however, a number of another situations, where the Schwarzschild geometry can be approximately applied: from strong fields of very slowly rotating black holes to the weak limit of normal stars. In our scenario, we use the advantage of the Schwarzschild geometry simplicity for an approximate description of gravity around object, which mimics a slowly rotating (more precisely non-rotating) compact neutron star. These stars are typically endowed with a dipole-type magnetic field, considered in our scenario. For sure, such a configuration can be precisely described by more complex geometries, e.g. Hartle-Thorne's [40] or Manko's [41]. Here, however, we restrict our attention to the illumination of basic properties of the charged toroidal configurations only; for this purpose the Schwarzschild geometry and test dipole magnetic field seems to be adequate.

In our illustrative scheme, we assume a sample of rather compact neutron star of the dimensionless radius $\mathcal{R} = 3$, being in geometrical units $\bar{\mathcal{R}} = 3\bar{M} = 3\bar{M}_\odot = 3 \times 1478 \text{ m} = \hat{\mathcal{R}}$, where the mass of the Sun in geometrical units $\bar{M} = \hat{M}_\odot \hat{G}/\hat{c}^2 = 1.99 \times 10^{30} \hat{G}/\hat{c}^2 \text{ kg} = 1478 \text{ m}$; the star is endowed with a dipole magnetic field with strength $\hat{\mathcal{B}} = 10^8 \text{ T}$ in the equatorial plane at the radius $r = \mathcal{R}$, corresponding to the dimensionless strength $\mathcal{B} = \bar{\mathcal{B}} \bar{M} \doteq 4.24 \times 10^{-8}$ and to the magnetic dipole moment $\mathcal{M} \doteq 4.2 \times 10^{-7}$ [42].

B. Fluid idealization—He compound

Questioning the kind of fluid forming the constructed tori, we must admit a considerable uncertainty. The introduced test bed model of the charged fluid does not conform with the widely presented accretion disc models. We assume the nonconductive fluid with global nonzero charge, contradicting the classic idea of plasma or dusty-plasma discs with high conductivity and quasi-neutrality. The pure dust grains seem to be not very convenient either because of its rather negligible pressure, which excludes it to be treated within the magnetohydrodynamic approach. Moreover, there is a considerable Coulombian repulsion between the charged dust grains, which we do not include in the presented model.

The possible scenario can be found in terms of the partly ionized helium—a proper mixture of neutral atoms or molecules with very low percentage of cations. The specific charge profile in a constructed torus, being by order far away from the proton one, can be interpreted as an average specific charge over a bulk of neutral particles bounding a cation, like in the mentioned helium composition. Such an idea, however, must be supported by an argument how to keep the charged helium species well locked among the neutral ones. This could be ensured by the here considered sufficiently high pressure and low temperature (high densities) in the fluid. Then, particle mean free path is smaller than atom size, and all the particles are “squeezed” enough to each other. The assumed rigid rotation of the fluid could support this scenario since in the $\omega = \text{const}$ case the circling fluid can sustain in the bulk hydrodynamic motion without the friction even for the required high densities.

The discussed partly ionized helium mixture is believed to form neutron stars atmospheres, also under the temperatures 10^7 K , magnetic fields 10^8 T and densities 10^4 kg m^{-3} considered here [45]. This kind of neutron star atmosphere could possibly serve as a source of matter for our tori being located very close to the star surface, although we are aware of the “high degree of idealization” of this scenario. There are, however, theoretical suggestions of the existence of (from neutron star surface spatially separated, but closely located) fluid structures—atmospheric gaseous shells [46].

Naturally, being focused on the region close to a neutron star, one can ask about the degenerate neutron gas as a

possible fluid forming the studied tori. The considered configurations could be imagined as being formed from bulk particles, each containing throng of neutrons and a proton, in accordance with the proper specific charge profile. However, we can see that due to very high densities of such a matter the tori constructed within the model would have to be extremely tiny in order to meet the condition of the test tori.

VI. CONCLUSIONS

Within the magnetohydrodynamic general-relativistic approach, we studied electrically charged toroidal structures encircling a central compact object endowed with a dipole magnetic field. This way we introduced a kind of direct continuation of our previous studies of charged toroidal structures [13,24,25]. Now, bringing the tori into new kind of background, we revealed new configurations of them and also updated the general solution of the mathematical concept of the model, currently being presented in the united analytic integral form.

Studying the problem, we confined ourselves to the case of gravito-electromagnetically test tori, i.e. mildly charged and lightweight, purely azimuthally rotating, requiring thus zero electrical conductivity. Along with these assumptions, we considered a perfect fluid satisfying the polytropic pressure–density relation and fixed the rotation with constant specific angular momentum distribution or with constant angular velocity (rigid rotation), both demanding a particular specific charge scattering throughout the torus.

We can briefly conclude that the charged toroidal structures can take shapes from rich topological family, existing not only in the equatorial plane as a single torus but also as two tori possibly coupled and joint through a cusp [47] or existing even out of the equatorial plane as a pair of off-equatorial tori. For comparison and better understanding of the charge influence, we briefly mentioned the family of electrically neutral tori (Polish doughnuts); we proved the absence of those in rigid rotation.

Along with the pure topological study of possible toroidal shapes, we also went through a basic astrophysical contextualization. By fitting the matter and fields

parameters, we proved that the toroidal structures can exist also within general astrophysical limits given by the maximal possible central pressure, density and temperature. For the purpose of a rough estimation, those had to be kept below the solar core values. We showed that within the considered model, the feasible tori must be relatively small in size, as compared with the central object, supporting also our conception of test tori.

For completeness, however, it is necessary to add that our discussion of the tori properties strongly depends on the choice of the charge correction function, being fixed *a priori*. A change of this function could lead to more or less interesting and realistic results, which can be part of a further investigation. We must also admit a certain incomprehension when questioning the origin of the matter circling in the constructed tori. This represents serious challenge for a future detailed study and matching, along with the update of the physics in the model, represented, e.g. by the considered thermodynamical setup. We are also interested in an improvement of the model itself, in the way of, e.g. inclusion of Coulombian interactions in the torus.

ACKNOWLEDGMENTS

The authors J. K., P. S., Z. S., V. K. and A. T. acknowledge the project “Albert Einstein Center for Gravitation and Astrophysics”, Czech Science Foundation GAČR Grant No. 14-37086G. The authors J. K., P. S. and Z. S. would also like to express their acknowledgment for the Institutional support of Faculty of Philosophy and Science, Silesian University in Opava; C. C. acknowledges financial support by the research project of the Czech Science Foundation GAČR Grant No. 14-07753P. We also acknowledge the COST Action MP1304 “Exploring fundamental physics with compact stars” (LD 15061). J. K. also expresses his gratitude for the great hospitality of the Harvard-Smithsonian Center for Astrophysics in Boston-Cambridge. V. K. acknowledges the support for the Czech-US collaboration from the Ministry of Education, Youth and Sports program Kontakt II (LH14049) titled “Spectral and Timing Properties of Cosmic Black Holes”.

-
- [1] J. Kovář, Z. Stuchlík, and V. Karas, *Classical Quantum Gravity* **25**, 095011 (2008).
 - [2] J. Kovář, O. Kopáček, V. Karas, and Z. Stuchlík, *Classical Quantum Gravity* **27**, 135006 (2010).
 - [3] O. Kopáček, V. Karas, J. Kovář, and Z. Stuchlík, *Astrophys. J.* **722**, 1240 (2010).
 - [4] M. Kološ, Z. Stuchlík, and A. Tursunov, *Classical Quantum Gravity* **32**, 165009 (2015).

- [5] Z. Stuchlík and M. Kološ, *Eur. Phys. J. C* **76**, 32 (2016).
- [6] C. Cremaschini, J.C. Miller, and M. Tassarotto, *Phys. Plasmas* **18**, 062901 (2011).
- [7] C. Cremaschini, J. Kovář, P. Slaný, Z. Stuchlík, and V. Karas, *Astrophys. J. Suppl. Ser.* **209**, 15 (2013).
- [8] C. Cremaschini, M. Tassarotto, and Z. Stuchlík, *Phys. Plasmas* **21**, 032902 (2014).

- [9] C. Cremaschini, M. Tassarotto, and Z. Stuchlík, *Phys. Plasmas* **21**, 052901 (2014).
- [10] C. Palenzuela, L. Lehner, O. Reula, and L. Rezzolla, *Mon. Not. R. Astron. Soc.* **394**, 1727 (2009).
- [11] B. Punsly, *Black Hole Gravito-hyromagnetics* (Springer-Verlag, Berlin, 2008).
- [12] L. Rezzolla and O. Zanotti, *Relativistic Hydrodynamics* (Oxford University Press, Oxford, England, 2013).
- [13] J. Kovář, P. Slaný, Z. Stuchlík, V. Karas, C. Cremaschini, and J. C. Miller, *Phys. Rev. D* **84**, 084002 (2011).
- [14] J. Frank, A. King, and D. Raine, *Accretion Power in Astrophysics* (Cambridge University Press, Cambridge, England, 2002).
- [15] M. Kozłowski, M. Jaroszyński, and M. A. Abramowicz, *Astron. Astrophys.* **63**, 209 (1978).
- [16] M. A. Abramowicz, M. Jaroszyński, and M. Sikora, *Astron. Astrophys.* **63**, 221 (1978).
- [17] Z. Stuchlík, P. Slaný, and S. Hledík, *Astron. Astrophys.* **363**, 425 (2000).
- [18] J. A. Font and F. Daigne, *Mon. Not. R. Astron. Soc.* **334**, 383 (2002).
- [19] L. Rezzolla, O. Zanotti, and J. A. Font, *Astron. Astrophys.* **412**, 603 (2003).
- [20] Z. Stuchlík, *Mod. Phys. Lett. A* **20**, 561 (2005).
- [21] P. Slaný and Z. Stuchlík, *Classical Quantum Gravity* **22**, 3623 (2005).
- [22] Z. Stuchlík, P. Slaný, and J. Kovář, *Classical Quantum Gravity* **26**, 215013 (2009).
- [23] H. Kučáková, P. Slaný, and Z. Stuchlík, *J. Cosmol. Astropart. Phys.* **01** (2011) 033.
- [24] J. Kovář, P. Slaný, C. Cremaschini, Z. Stuchlík, V. Karas, and A. Trova, *Phys. Rev. D* **90**, 044029 (2014).
- [25] P. Slaný, J. Kovář, Z. Stuchlík, and V. Karas, *Astrophys. J. Suppl. Ser.* **205**, 3 (2013).
- [26] P. Goldreich and W. H. Julian, *Astrophys. J.* **157**, 869 (1969).
- [27] J. M. Cohen and E. T. Toton, *Astrophys. Lett.* **7**, 213 (1971).
- [28] L. Mestel, *Nature (London) Phys. Sci.* **233**, 149 (1971).
- [29] R. N. Henriksen and D. R. Rayburn, *Mon. Not. R. Astron. Soc.* **166**, 409 (1974).
- [30] C. W. Misner, K. S. Thorne, and J. A. Wheeler, *Gravitation* (Freeman, San Francisco, 1973).
- [31] C. Cremaschini and M. Tassarotto, *Eur. Phys. J. Plus* **126**, 63 (2011).
- [32] In physical SI units, we have the relation $\hat{p} = \hat{k}_B / \hat{m}_u \hat{p} \hat{T}$, where the Boltzmann constant $\hat{k}_B \doteq 1.38 \times 10^{-23}$ J/K and the atomic unit mass $\hat{m}_u \doteq 1.66 \times 10^{-27}$ kg.
- [33] A. R. Prasanna and S. Sengupta, *Phys. Lett. A* **193**, 25 (1994).
- [34] P. Bakala, E. Šrámková, Z. Stuchlík, and G. Török, *Classical Quantum Gravity* **27**, 045001 (2010).
- [35] A similar approach was used also in the case of a globally neutral magnetized fluid (plasma) circling in strong gravitational field and toroidal magnetic field [36].
- [36] S. S. Komissarov, *Mon. Not. R. Astron. Soc.* **368**, 993 (2006).
- [37] Rewriting relation (63) into the form $e^h U_t = \text{const}$, we can note the correspondence with one of the important results of the work [29]—relation (20). The correspondence is obvious; nevertheless, the authors consider a little bit different scenario from the one presented here. For instance, the differences are the rotation of the dipole magnetic field, constant specific charge of the matter, rigid co-rotation of the matter with the magnetic field, nonzero conductivity and a slightly different thermodynamical setup.
- [38] In the case $\ell = \text{const}$, the angular term in the pressure equations (38) vanishes, and in the case $\omega = \text{const}$, we have the condition $\omega = \omega(\ell)$ satisfied. Thus, in both the cases we can advantageously use the solution of the pressure equations in the united form (53), assuming that the correction function must be chosen as a function of \mathcal{A}_ϕ .
- [39] Note that in the original works of M. Abramowicz and his co-workers, the potential \tilde{H} is denoted as W .
- [40] J. B. Hartle and K. S. Thorne, *Astrophys. J.* **153**, 807 (1968).
- [41] V. S. Manko, E. W. Mielke, and J. D. Sanabria-Gómez, *Phys. Rev. D* **61**, 081501 (2000).
- [42] Note that the masses and radii of neutron stars are generally assumed in the ranges $1 \hat{M}_\odot \leq \hat{M} \leq 3 \hat{M}_\odot$ and $3\hat{M} \leq \hat{R} \leq 10\hat{M}$ [43]; magnetic fields reach their strengths $\hat{B} = 10^{10}$ T [44]. The precise determination of the mentioned limits, however, is still of high interest, being very complex, dependent on the considered equation of state, etc.
- [43] J. M. Lattimer and M. Prakash, *Science* **304**, 536 (2004).
- [44] J. M. Lattimer and M. Prakash, *Phys. Rep.* **442**, 109 (2007).
- [45] K. Mori and J. S. Heyl, *Mon. Not. R. Astron. Soc.* **376**, 895 (2007).
- [46] M. Wielgus, W. Kluźniak, A. Sadowski, R. Narayan, and M. Abramowicz, *Mon. Not. R. Astron. Soc.* **454**, 3766 (2015).
- [47] The coupled simultaneously existing tori with a common cusp discussed here reminds us of the similar so-called ring equilibrium configuration of the neutral fluid discussed in papers [48,49], there caused by the rotation of the central object and the chosen different angular momentum of the multiple tori. Here, a different physical ground for this effect occurs—the additional electromagnetic interaction.
- [48] D. Pugliese and Z. Stuchlík, *Astrophys. J., Suppl. Ser.* **221**, 25 (2015).
- [49] D. Pugliese and Z. Stuchlík, *Astrophys. J., Suppl. Ser.* **223**, 27 (2016).